AD-A126 117 THE AXISYMMETRIC INSTABILITY OF A SELF-PINCHED BEAM WITH A ROUNDED RADIAL.. (U) NAVAL SURFACE WEAPONS CENTER SILVER SPRING MD H C CHEN ET AL. DEC 82 NSWC/TR-83-14 1/1

UNCLASSIFIED SBI-AD-F500 141 F/G 20/7 NL

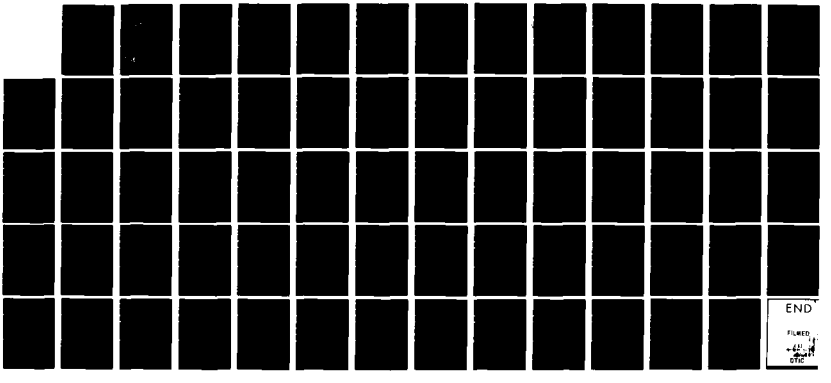

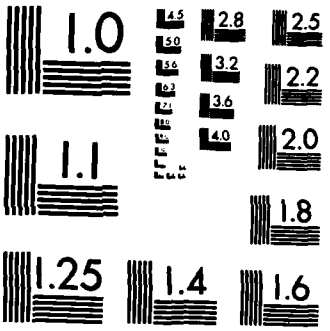

NSWC TR 83-14
PLASMA PHYSICS PUBLICATION NO. 82-11

THE AXISYMMETRIC INSTABILITY OF A SELF-PINCHED BEAM WITH A ROUNDED RADIAL DENSITY PROFILE

BY H. C. CHEN,
H. S. UHM

RESEARCH AND TECHNOLOGY DEPARTMENT

DECEMBER 1982

Approved for public release, distribution unlimited.

NAVAL SURFACE WEAPONS CENTER
Dahlgren, Virginia 22448 • Silver Spring, Maryland 20910

UNCLASSIFIED

SECURITY CLASSIFICATION OF THIS PAGE (When Data Entered)

REPORT DOCUMENTATION PAGE		READ INSTRUCTIONS BEFORE COMPLETING FORM
1. REPORT NUMBER NSWC TR 83-14	2. GOVT ACCESSION NO. AD-A126 117	3. RECIPIENT'S CATALOG NUMBER
4. TITLE (and Subtitle) THE AXISYMMETRIC INSTABILITY OF A SELF-PINCHED BEAM WITH A ROUNDED RADIAL DENSITY PROFILE		5. TYPE OF REPORT & PERIOD COVERED 6. PERFORMING ORG. REPORT NUMBER
7. AUTHOR(s) H. C. Chen and Han S. Uhm		8. CONTRACT OR GRANT NUMBER(s)
9. PERFORMING ORGANIZATION NAME AND ADDRESS Naval Surface Weapons Center (Code R41) White Oak Silver Spring, MD 20910		10. PROGRAM ELEMENT, PROJECT, TASK AREA & WORK UNIT NUMBERS 61152N; ZR00001; ZR01109; R01AA400
11. CONTROLLING OFFICE NAME AND ADDRESS		12. REPORT DATE December 1982 13. NUMBER OF PAGES 68
14. MONITORING AGENCY NAME & ADDRESS(if different from Controlling Office)		15. SECURITY CLASS. (of this report) UNCLASSIFIED 15a. DECLASSIFICATION/DOWNGRADING SCHEDULE

16. DISTRIBUTION STATEMENT (of this Report)

Approved for public release; distribution unlimited.

17. DISTRIBUTION STATEMENT (of the abstract entered in Block 20, if different from Report)

18. SUPPLEMENTARY NOTES

19. KEY WORDS (Continue on reverse side if necessary and identify by block number)

Self-pinched Beam
Radial Density Profile

20. ABSTRACT (Continue on reverse side if necessary and identify by block number)

The axisymmetric perturbations (sausage and hollowing modes) of an intense relativistic self-pinched electron beam propagating in a resistive plasma background are studied, especially for a beam with rounded radial density profile. The Bennett profiles are assumed for both the equilibrium beam current $J_b(r) = J_b(0)\ (1 + r^2/R_b^2)^{-2}$ and plasma return current $J_p(r) = -f\ J_b(0)\ (1 + r^2/R_p^2)^{-2}$, where R_b and R_p are the characteristic radii of the beam and

DD FORM 1 JAN 73 1473 EDITION OF 1 NOV 65 IS OBSOLETE
S/N 0102-LF-014-6601

UNCLASSIFIED

SECURITY CLASSIFICATION OF THIS PAGE (When Data Entered)

plasma return currents respectively. It is further assumed that the electric conductivity $\sigma(r)$ of the plasma channel is proportional to the return current. For a paraxial electron beam with complete space-charge neutralization by the ambient plasma, the axisymmetric modes can be destabilized by the phase lag between the magnetic field and beam current, even without the plasma return current.

The plasma return current significantly modifies the growth rate of the instability such that the ratio of plasma to beam current ($-I_p/I_b = f\, R_p^2/R_b^2$) largely determines the stability character of the beam. Furthermore, for the same fractional current neutralization f, the modes are highly unstable for smaller ratio of plasma to beam radius R_p/R_b. As comparing to the resistive hose instability, the growth rates for hollowing mode could be larger than those of hose mode, while the sausage mode is much stabler than the hose mode. Stability properties are illustrated in detail for various system parameters.

FOREWORD

The axisymmetric perturbations (sausage and hollowing modes) of an intense relativistic self-pinched electron beam propagating in a resistive plasma background are studied, especially for a beam with rounded radial density profile. The Bennett profiles are assumed for both the equilibrium beam current $J_b(r) = J_b(0)\ (1 + r^2/R_b^2)^{-2}$ and plasma return current $J_p(r) = -f\ J_b(0)\ (1 + r^2/R_p^2)^{-2}$, where R_b and R_p are the characteristic radii of the beam and plasma return currents respectively. It is further assumed that the electric conductivity $\sigma(r)$ of the plasma channel is proportional to the return current. For a paraxial electron beam with complete space-charge neutralization by the ambient plasma, the axisymmetric modes can be destabilized by the phase lag between the magnetic field and beam current, even without the plasma return current.

The plasma return current significantly modifies the growth rate of the instability such that the ratio of plasma to beam current ($-I_p/I_b = f\ R_p^2/R_b^2$) largely determines the stability character of the beam. Furthermore, for the same fractional current neutralization f, the modes are highly unstable for smaller ratio of plasma to beam radius R_p/R_b. As comparing to the resistive hose instability, the growth rates for hollowing mode could be larger than those of hose mode, while the sausage mode is much stabler than the hose mode. Stability properties are illustrated in detail for various system parameters.

Approved by:

Ira M. Blatstein

IRA M. BLATSTEIN, Head
Radiation Division

CONTENTS

Section		Page
I	INTRODUCTION	1
II	EQUILIBRIUM STATE	5
III	STABILITY ANALYSIS	11
IV	CONCLUSIONS	31
V	ACKNOWLEDGEMENTS	33

ILLUSTRATIONS

Figure		Page
1	THE GROWTH REGION FOR THE SAUSAGE MODE WITH $R_p = R_b$ IN THE f - Ω SPACE	34
2	THE GROWTH RATE OF NON-OSCILLATORY SAUSAGE MODE OSCILLATION VERSUS f FOR THE ROUNDED AND FLAT-TOPPED BEAMS	35
3	THE GROWTH RATE OF THE SAUSAGE MODE VERSUS Ω^2 FOR VARIOUS f FOR THE FLAT-TOPPED BEAM	36
4	GROWTH RATE $Im(\omega)$ AND REAL EIGENFREQUENCY $R_e(\omega)$ VERSUS Ω^2 FOR THE SAUSAGE MODE OF A BENNETT BEAM WITH $R_p = R_b$ FOR VARIOUS f	37
5	THE UNSTABLE REGION OF THE SAUSAGE MODE OF THE BENNETT BEAM IN THE f_{eff} - Ω SPACE FOR R_p/R_b = 2, 4, 6 RESPECTIVELY	38
6	GROWTH RATE $Im(\omega)$ AND REAL EIGENFREQUENCY $R_e(\omega)$ VERSUS Ω^2 FOR THE SAUSAGE MODE OF A BENNETT BEAM WITH $R_p = 2\ R_b$ FOR VARIOUS f_{eff}	39
7	THE UNSTABLE REGION OF THE SAUSAGE MODE OF THE BENNETT BEAM IN THE f_{eff} - Ω SPACE FOR R_p/R_b = 0.9, 0.5, AND 0.1 RESPECTIVELY	40
8	GROWTH RATE $Im(\omega)$ AND REAL EIGENFREQUENCY $Re(\omega)$ VERSUS Ω^2 FOR THE SAUSAGE MODE OF A BENNETT BEAM WITH $R_p = 0.5\ R_b$ FOR VARIOUS f_{eff}	41
9	NONOSCILLATORY GROWTH REGION FOR A BENNETT BEAM IN THE f_{eff} - R_p/R_b SPACE	42
10	THE GROWTH REGION FOR THE HOLLOWING MODE WITH $R_p = R_b$ IN THE f - Ω SPACE	43
11	THE GROWTH RATE OF THE HOLLOWING MODE VERSUS Ω^2 FOR VARIOUS f FOR THE FLAT-TOPPED BEAM	44
12	GROWTH RATE $Im(\omega)$ AND REAL EIGENFREQUENCY $Re(\omega)$ VERSUS Ω^2 FOR THE HOLLOWING MODE OF A BENNETT BEAM WITH $R_p = R_b$ FOR VARIOUS f	45

ILLUSTRATIONS (Cont.)

Figure		Page
13	THE UNSTABLE REGION OF THE HOLLOWING MODE OF THE BENNETT BEAM IN THE $f_{eff} - \Omega$ SPACE FOR R_p/R_b = 1.1, 2, 4, RESPECTIVELY	46
14	GROWTH RATE Im(ω) AND REAL EIGENFREQUENCY Re(ω) VERSUS Ω^2 FOR THE HOLLOWING MODE OF A BENNETT BEAM WITH $R_p = 2\ R_b$ FOR VARIOUS f_{eff}	47
15	THE UNSTABLE REGION OF THE HOLLOWING MODE OF THE BENNETT BEAM IN THE $f_{eff} - \Omega$ SPACE FOR R_p/R_b = 0.9, 0.5, 0.1, RESPECTIVELY . . .	48
16	GROWTH RATE Im(ω) AND REAL EIGENFREQUENCY Re(ω) VERSUS Ω^2 FOR THE HOLLOWING MODE OF A BENNETT BEAM WITH $R_p = 0.5\ R_b$ FOR VARIOUS f_{eff}	49

I. Introduction

There has been considerable interest in recent years in the propagation of high-energy self-pinched relativistic electron beam in the highly resistive plasma medium. Naturally, the equilibrium and stability properties of the electron beam become one of the important subjects under investigation. The resistive hose instability appears to be the most serious magnetohydrodynamic instability for a beam in a resistive plasma channel and has been studied extensively by many authors.[1-3] Nevertheless, the axisymmetric oscillations could expell the beam from its channel and plague early beam propagation.[4] It is the purpose of this paper to examine the importance of the axisymmetric modes in comparison with the hose mode. The axisymmetric perturbations of an intense self-pinched relativistic electron beam propagating in the plasma background have been studied previously by many workers both analytically[5,6] and numerically.[7,8] Recently Uhm and Lampe developed a self-consistent theory[1,9] to derive the dispersion relation for a flat-topped radial density profile electron beam. This paper is an improved version of the previous study, including the influence of the rounded beam density profile on the axisymmetric modes. It has been understood that the flat-topped electron beam has the feature of unbounded linear growth rate for axisymmetric oscillations because all the beam electrons are assumed to have the same natural oscillation frequency which resonants with the wave. As we know in the real world, the beam contains electrons of all energies from the smallest up to the maximum possible energy which is equal to the kinetic energy of the accelerated electron. The electrons at different energy level oscillates with different frequencies and radii, thus the unharmonic beam electrons at different radial position exhibit different betatron frequency and resonant locally with the waves. Electrons with an excess of energy will move with

a greater radius and electrons with less energy oscillates around smaller radius. Therefore, each electron automatically chooses the appropriate phase necessary for their interaction with perturbed waves. This phase mixing is a damping mechanism for oscillation which prevents perturbation from growing to infinity.

From the thermal equilibrium calculations of the intense relativistic electron beam, it was found that the radial density profile for a nonrotating electron beam has the familiar Bennett equilibrium as derived originally by Bennett.[10] For the choice of the thermal distribution function, the beam temperature profile and the axial velocity profile are uniform in the radial direction.[11] For the matter of practical interest, we assume the beam flow is paraxial, such that all the beam particles have nearly the same axial velocity, and the transverse energy is much smaller than that in the axial direction. For the type of beam we consider here, the equilibrium beam current can very well be represented by the Bennett profile

$$J_b(r) = J_b(0)/(1 + r^2/R_b^2)^2 \qquad (1)$$

where R_b is the characteristic beam radius.

The resistive plasma background responds the beam current with a plasma return current which strongly influences the stability behavior of the beam. A small transverse displacement of thc beam can separate the beam from the return current which eventually causes the instability. For simplicity we assume the plasma background supplies enough ions to neutralize the beam electrons completely. Although the radial profile of the return current is determined by the electrical conductivity $\sigma(r)$ which relies heavily on the properties of the ambient plasma and experimental condition, for the time

being, it is assumed throughout this paper that the equilibrium plasma return current $J_p(r)$ and electrical conductivity $\sigma(r)$ have also the Bennett profile like

$$J_p(r) = -f\, J_b(0)/(1 + r^2/R_p^2)^2 \tag{2}$$

and

$$\sigma(r) = \sigma(0)/(1 + r^2/R_p^2)^2 \tag{3}$$

where the characteristic beam radius R_p can be greater or smaller than R_b depending on the nature of the background plasma such as the ambient pressure and other physical properties. f is the ratio of beam current to plasma current at the beam axis

$$f \equiv -J_p(0)/J_b(0) \ . \tag{4}$$

If the above mentioned equilibrium current configurations are used, then the effective current neutralization would be determined by the ratio of plasma to beam current which has the value

$$f_{eff} \equiv -I_p/I_b = f\, R_p^2/R_b^2 \tag{5}$$

The influence of the steady return current on the axisymmetric perturbations depends largely on the extent of plasma current profile overlapped with the beam current. By varying R_b and R_p, the effective current neutralization not only denotes the measure of roundness of the beam but also represents the degree of

overlap between beam and plasma current profiles. It is an important parameter used later to describe the effect of the current profiles on the instability.

In the sections which follow, the equilibrium properties of a self-pinched electron beam with a steady plasma return current are discussed in Section II, the necessary condition for radial confinement of the electron beam is examined. The standard linearized Vlasov-Maxwell treatments are summarized in Section III. An integro-differential eigenvalue equation is obtained for the general rounded beam case, making use of the energy group model. The most important source term, namely the perturbed beam current for the rounded beam is also derived. For the purpose of comparison to the previous results, an integral form of an approximate dispersion relation is obtained for the general rounded beam. For the special case where the electrical conductivity, the beam and plasma return currents all have the Bennett profile, numerical results are obtained for various system parameters such as f, R_p and R_b. Stability properties for the sausage and hollowing modes are illustrated and discussed in great detail. Finally, the growth rates of the axisymmetric modes are compared to those of the hose instability and the conclusions are drawn in Section IV.

II. Equilibrium state

Let us consider the steady state of an infinitely long intense relativistic self-pinched electron beam propagating in a resistive background plasma. The beam dynamic properties are described by the Vlasov-Maxwell Theory. In the following analysis, the cylindrical polar coordinates (r, θ, z) are used with the z-axis along the axis of symmetry. In steady state ($\partial/\partial t = 0$) all the beam equilibrium quantities are assumed to be azimuthally symmetric ($\partial/\partial \theta = 0$) and infinitely long and uniform in the axial direction ($\partial/\partial z = 0$). The beam with net current I is assumed to satisfy the following relationship[12]

$$I/I_a = \nu/\gamma = I/17000\ \beta\gamma << 1 \tag{6}$$

where ν is Budker's parameter representing the number of electrons per classical electron radius length of the beam, $V_b = \beta c$ is the characteristic beam electron axial velocity, γ is the relativistic factor of the beam particle and I_a is the Alfven-Lawson limiting current. The beam electrons motion can be taken to be paraxial ($P_z^2 >> P_r^2 + p_\theta^2$) where P_i denotes the three components of the canonical angular momentum in i direction respectively. The axial velocity is very large compared to the transverse velocity and is considered to be a constant. In this regime, the equilibrium properties of an electron beam can be described by a velocity distribution function of the form

$$f_b = F\ (H - \gamma_0 mc^2)\ \delta\ (P_z - P_b) \tag{7}$$

where H is the total energy, P_z is the axial canonical momentum. The single

particle constants of motions in the equilibrium fields are given by

$$H = (m^2c^4 + c^2p^2)^{\frac{1}{2}}$$

$$P_z = p_z - e\,A_z\,(r)/c$$

where $\gamma_b \equiv (1 - \beta^2)^{-\frac{1}{2}}$ and $\beta \equiv v_b/c$ are the standard relativistic quantities, m and v_b are the rest mass and the velocity of the beam electron, c is the velocity of light in vacuum, γ_0 and P_b are constants, $A_z(r)$ is the axial component of vector potential for the equilibrium azimuthal self-magnetic field. There is no externally applied magnetic field in the self-pinched beam case so that $P_\theta = 0$. As a result, we can assume that f_b is not a function of P_θ as shown in (7). For the nonrotating beam, the vector potential $\underline{A}\,(r)$ has only the axial component $A_z(r)$ which can be determined self-consistently from the z component of the Ampere's law

$$\frac{1}{r}\frac{\partial}{\partial r}\,(rB_\theta) = -4\pi e\beta\left[\,n_b(r) - n_p(r)\right] \tag{8}$$

where $n_b(r)$ is the radial number density distribution of the electron beam, $n_p(r)$ is not the actual number density but related to the plasma return current by $J_p(r) = -e\beta c\, n_p(r)$. and by definition

$$B_\theta = -\partial A_z(r)/\partial r \tag{9}$$

where in deriving Eq. (8) the paraxial beam approximation has been used. All the electrons have the same axial velocity $V_z = \beta c$ and the transverse velocity of the beam electron is small compared with the axial velocity. Eq. (8) can

be used to calculate equilibrium azimuthal self-magnetic field self-consistently for any net current in the system. The relationship can be further related to the squared betatron frequency as

$$\omega_\beta^2(r) \equiv -e\beta B_\theta(r)/\gamma_b mr$$

$$= (4\pi e^2\beta^2/\gamma_b mr^2)\int_0^r dr' r' \left[n_b(r') - n_p(r')\right] \tag{10}$$

where ω_β is the usual betatron frequency which characterizes the electron oscillations.

If the beam and plasma return currents have the assumed Bennett profile as in Eqs. (1) and (2), then Eq. (10) gives the value after integration

$$\omega_\beta^2\ (r) = 0.5\ \omega_{pb}^2\beta_b^2\ \left[1/(1+r^2/R_b^2) - f/(1+r^2/R_p^2)\right] \tag{11}$$

where $\omega_{pb} \equiv (4\pi n_b(0)e^2/\gamma_b m)^{\frac{1}{2}}$ is the beam plasma frequency at axis. It is important to point out that ω_β is a function of r except in the special case of a flat-topped beam which has the constant value; i.e.,

$$\omega_\beta^2 = 0.5\ \omega_{pb}^2\beta_b^2\ (1-f) \tag{12}$$

This is the most important distinction between the rounded and flat-topped beams, which gives, by no surprise, two complete different pictures in the linear perturbation analysis. In short, the growth rate for axisymmetric perturbations goes to infinity as $\Omega \to \omega_\beta$ for the flat-topped beam, because the pinch force is harmonic. All the beam electrons are able to resonate with the wave at the same frequency. On the other hand, because the pinch

force is anharmonic for the rounded beam, the electrons have a wide variety of betatron frequencies which could damp the oscillation by phase mixing mechanism. It could have only radially localized wave-particle resonance, so that the growth rate is finite, which will become more obvious later.

As a matter of fact, if the squared betatron frequency is negative at certain radius r, then the equilibrium fails, and the beam is blown apart. Therefore, the radial confinement for the equilibrium state requires at least $\omega_\beta^2(r) > 0$ for any radius r inside the beam. This assures that the magnetic focussing force is pinching the beam; otherwise, the beam will be hollowing out and eventually will become an annular beam. Since we have assumed in the beginning that the equilibrium beam current has the Bennett profile, the minimum requirement for such equilibrium profile to exist needs $\omega_\beta^2(r) > 0$, which leads to

$$f < (1 + r^2/R_p^2)/(1 + r^2/R_b^2) \tag{13}$$

For the case of $R_b > R_p$, the fractional current neutralization f is bounded by

$$f < 1 \quad , \qquad R_p < R_b, \tag{14}$$

so that the beam current $J_b(r)$ is peaked on axis. However, if $R_b < R_p$, we obtain from Eq. (13) that

$$f < (R_b/R_p)^2 \quad , \qquad R_b < R_p, \tag{15}$$

which is equivalent to $f_{eff} < 1$. Note that in the limit where $R_b = R_p$, both Eqs. (14) and (15) yield the same condition, namely $f < 1$, which also applies to the flat-topped beam case.

Next let us consider an electron beam with a "loss-cone" distribution function

$$f_b = (n_b/2\pi\gamma_b m)\ \delta\ (H - \gamma_0 mc^2)\ \delta\ (P_z - P_b). \tag{16}$$

Integration of (16) in the $\underline{P}$ space, according to definition, leads to a density distribution with flat-topped radial profile

$$n_b(r) = \begin{cases} n_b & \text{for } 0 \leq r < R_b \\ 0 & \text{for } R_b < r \end{cases} \tag{17}$$

where $n_b(r)$ is the equilibrium beam density profile and R_b is defined as the effective beam radius such that the number of electrons per unit length of the beam has

$$N_b \equiv 2\pi \int_0^\infty dr\ r\ n_b(r) = \pi\ R_b^2 n_b \tag{18}$$

Note that the beam with flat-topped or Bennett profiles carry essentially the same amount of total current, which is very important when we compare the growth rates in both cases later on.

In the energy group model a beam has been subdivided into groups of particles with the same value of energy. By use of Eq. (7) the beam current

profile can be expressed by definition as

$$J_b(r) = 2\pi\gamma_b me\beta c \int_{\Phi_0(r)}^{\infty} dU\ F\ (U + \gamma_b mc^2) \tag{19}$$

where $U \equiv H - \gamma_b mc^2$ is the effective transverse energy and $\Phi_0(r) \equiv e\beta A_z(r)$, which appeares in the lower limit of integration, is the minimum possible value of U necessary for an electron at r. Thus, the beam can be considered as a superposition of many components with different transverse energy

$$J_b(r) = \int_0^{\infty} dU\ F\ (U + \gamma_b mc^2)\ J_0(r, U) \tag{20}$$

where each component has the equilibrium current density profile like

$$J_0(r, U) = \begin{cases} -2\pi\gamma_b me\beta c & r < R\ (U) \\ 0 & r > R\ (U) \end{cases} \tag{21}$$

where R(U) is the maximum radius for an electron with energy U.

III. Stability Analysis

A. Linear Perturbations

In this section, we use the linearized Vlasov-Maxwell equations to investigate the axisymmetric perturbations (m = 0) where m is the azimuthal harmonic number. We follow a normal mode approach by assuming that all the axisymmetric perturbed quantities vary with z and t according to

$$\delta\Phi(\underline{x},t) = \delta\Phi(r) \exp\left[- j(\omega\tau + \Omega z/v_z)\right] \tag{22}$$

where the oscillating angular frequency ω is assumed to be complex with $Im(\omega) > 0$. The variables τ and Ω are defined by

$$\tau \equiv t - z/v_z$$

and $\Omega \equiv \omega - kv_z$.

Where z and t are the axial position and time in the laboratory frame, k is the axial wavenumber. Since all the beam electrons have nearly the same axial velocity for the paraxial beam we consider here, it is more convenient to use z and τ as independent variables than the normal use of z and t. Thus Ω is the Doppler-shifted eigenfrequency seen by a beam electron, $V_b\tau$ is a measure of the distance of a particular segment from the head of the beam. If each beam segment is taken to oscillate at a fixed real frequency Ω then the solution for complex ω can be solved mathematically from the dispersion relation. Physically $Im(\omega)$ represents the growth rate of the wave as we move backward from the head of the beam.

After Fourier decomposing the Maxwell equations, it is straightforward to show that for the case of long wave length ($k R_b << 1$) and low frequency ($\omega R_b << c$) regime the eigenvalue equation for the perturbed field $\delta\phi$ has the form

$$\frac{1}{r} \frac{\partial}{\partial r} r \frac{\partial}{\partial r} \delta\phi + \frac{4\pi\sigma\omega i}{c^2} \delta\phi = - \frac{4\pi}{c} \delta J_b(r) \tag{23}$$

where σ is the electrical conductivity of the plasma channel and the Vlasov perturbed beam current contribution $\delta J_b(r)$ is defined as

$$\delta J_b(r) = - e \int v_z \delta f_b (r, \underline{p}) d\underline{p} . \tag{24}$$

where $\delta f_b(r,\underline{p})$ is to be calculated from the integration of the linearized Vlasov equation. According to the energy group model in Eq. (20) one can express the perturbed beam current as

$$\delta J_b(r) = \int_0^\infty dU \; F(U + \gamma_b mc^2) \delta J_0(r,U). \tag{25}$$

By use of Eq. (19) one can derive the following relationship

$$Fd\Phi_0(R)/dR = (1/2\pi\gamma_b me\beta c) \partial J_b(R)/\partial R \tag{26}$$

Substituting Eq. (26) into Eq. (25) for change of variables, one can finally write down the perturbed beam current below

$$\delta J_b(r) = (1/2\pi\gamma_b me\beta c) \int_r^\infty dR \quad \frac{dJ_b(R)}{dR} \quad \delta J_0(r,R) \tag{27}$$

If the plasma is a perfect conductor with infinite conductivity, all the beam particles which initially lie on a magnetic field line should continue to do so, and when they move the field must in some sense be carried along by the conductor. This is what Alfvén[13] expressed dramatically by saying that the field and fluid were "frozen together". On the contrary, if the plasma resistivity is significant, there is a phase lag between the beam oscillations and the magnetic restoring force. This magnetic decay force prevents the field line from following the beam oscillation which causes the instability to grow. This driving force is well represented by the second term of Eq. (23). The plasma return current influences the structure of the equilibrium beam current and vise versa which will be discussed in a separate paper later on. What we concern here is both currents with different radial profile strongly effect the perturbed beam current which in turn goes to Eq. (23) to determine the perturbed field. This is a major driving force for the axisymmetric perturbations. We will concentrate to derive the most important quantity, namely the perturbed beam current for the rounded beam.

Recall that for the loss-cone distribution as in Eq. (16) the corresponding beam density profile is known to be flat-topped as shown in Eq. (17). To solve the linearized Vlasov equation for the perturbed distribution function $\delta f_b(\underline{x},\underline{p},t)$, one can do the orbit integration along the unperturbed particle orbits, using the method of characteristic. From this standard Vlasov analysis and using a variational approximation method, an approximate dispersion relation can be obtained with the help of the trial eigenfunction of the form

$$\delta\phi_n(r) = \sum_{j=0}^{n} A_j (r/R_b)^{2j} \qquad 0 \le r \le R_b \tag{28}$$

where n is the radial mode number. We will mainly be interested in the lower order number modes, namely n = 1 and 2 which are believed to be the most important perturbations. For n = 1 which is identified as sausage mode, the eigenfunction has the simple form

$$\delta\phi_1(r) = \begin{cases} A_0(1 - r^2/R_b^2) & 0 \le r < R_b \\ 0 & R_b \le r \end{cases} \tag{29}$$

which is a self-consistent solution to Eq. (23). The perturbed beam current density as defined in Eq. (24) can be integrated with the help of eigenfunction (29). This standard procedure but tedious operation gives the final result for the axial component of the perturbed current density like

$$\delta J_b(r) = \frac{c\beta^2}{4\pi} \frac{1}{r} \frac{\partial}{\partial r} \left(r \frac{\omega_{pb}^2(r)}{\Omega^2 - \omega_\beta^2} \frac{\partial}{\partial r} \delta\phi(r) \right) \tag{30}$$

as given in Eq. (32) of reference 5, where the plasma frequency $\omega_{pb}(r)$ is defined for the flat-topped beam by

$$\omega_{pb}^2(r) = \begin{cases} 4\pi n_b(0) e^2/\gamma_b m & 0 < r < R_b \\ 0 & R_b < r \end{cases} \tag{31}$$

Similarly, let us consider next the radial mode number n = 2 which is known as hollowing mode. The name "hollowing" comes because the perturbation can indeed reduce the beam density on axis, leading to a hollow beam profile. The eigenfunction for n = 2 has been given by

$$\delta\phi_2(r) = \begin{cases} A_0(1 - 4r^2/R_b^2 + 3r^4/R_b^4) & 0 \le r \le R_b \\ 0 & R_b < r \end{cases} \tag{32}$$

After some tedious algebraic manipulations as demonstrated in reference (5), the z component of the perturbed current density finally becomes

$$\delta J_b(r) = \frac{c\beta^2}{4\pi} \frac{1}{r} \frac{\partial}{\partial r} \left(r \frac{\partial \delta\phi}{\partial r} \frac{\omega_{pb}^2(r)}{\Omega^2 - \omega_\beta^2} \left(1 + \frac{18\ \omega_\beta^2}{\Omega^2 - 4\omega_\beta^2}\right)\right) \tag{33}$$

Eqs. (30) and (33) display explicitly the intrinsic singularity at $\Omega^2 = \omega_\beta^2$ for wave-particle resonance. Moreover, it is further noticed that the hollowing mode has another singularity at second harmonic betatron frequency too; i.e., $\Omega^2 = 4\omega_\beta^2$. For the same token, one can expect more singularities at higher harmonic frequencies for higher order modes. Since ω_β is single-valued for the flat-topped beam, every electron can be in resonance at the same frequency and there is no limitation for the instability to grow. Therefore, it is almost impossible for a flat-topped beam to propagate in any medium. Fortunately as we shall see later because the beam is rounded, the nature is not going to be so cruel to allow the instability to grow indefinitely.

For the obvious reason, we are going to consider the importance of the influence of rounded radial density profile on axisymmetric perturbations. As we mentioned earlier, the betatron frequency is a function of radius r as long as the beam profile is rounded. It is very common to have energy spread for a high energy beam even right after coming out of the accelerator. In nature, it always represents an oscillation in energy about the equilibrium value. As long as the energy exceeds the equilibrium energy, the electron will travel

in orbit of larger radii, conversely, it will have smaller orbit at lower energy. The electrons reside on each infinitesmal Δr can have approximately constant ω_β with which they resonate locally. Therefore, it is quite reasonable to extend from the previous results for the flat-topped beam profile to include the rounded beam profile effect. To investigate the sausage and hollowing modes for the rounded beam, we have to derive first the perturbed beam current and the associated eigenfunction for each mode which are described below separately.

1. Sausage mode (n = 1)

It is evident that a beam with rounded radial density profile can be subdivided into groups of particles with the same value of energy, and in addition, it can also be sliced into components with different radii. As pointed out in Eq. (30), each energy group designated by R gives its perturbed axial current density for the n = 1 sausage mode

$$\delta J_0(r,R) = 2\pi e^2 c\beta^2 \frac{1}{r}\frac{\partial}{\partial r}\left\{ r \frac{\partial \delta\phi}{\partial r} \quad \frac{dJ_b(R)/dR}{\Omega^2 - \omega_\beta^2(R)} \right\} \tag{34}$$

where $\delta J_0(r,R)$ should be a continuous function on $0 < r < R$ and vanish smoothly at r = 0. Substituting Eq. (34) into Eq. (27) for summing up each individual component of the perturbed beam current, we have finally the result for the axial perturbed beam current like

$$\delta J_b(r) = \frac{e\beta}{\gamma m} \frac{1}{r} \frac{\partial}{\partial r} \left\{ r \int_r^\infty dR \; \frac{dJ_b(R)/dR}{\Omega^2 - \omega_\beta^2} \frac{\partial \delta\phi}{\partial r} \right\} \tag{35}$$

The corresponding eigenfunction is given by

$$\delta\phi_1(r) = \int_r^\infty dR \; A_0 \; (1 - r^2/R^2) \; dJ_b(R)/dR \tag{36}$$

Note that the intrinsic singularity at $\Omega = \omega_\beta$ in Eq. (30) for the flat-topped case has been replaced by the integration over R space which eventually gives a logarithmic singularity. Because of this, the growth rate is no longer unbounded as in the flat-topped case. The natural oscillation frequency ω_β varies for different electrons at different radius r, so that there is no single frequency Ω for which the entire beam electrons can resonate with the wave.

2. Hollowing mode (n = 2)

Accordingly, after considering the n = 1 sausage mode, likewise we can easily derive, based on the same theory, the perturbed current density and corresponding trial eigenfunction for the n = 2 hollowing mode. By use of Eqs. (32) and (33), one can obtain the perturbed beam current which has the axial component

$$\delta J_b(r) = \frac{e\beta}{\gamma m}\frac{1}{r}\frac{\partial}{\partial r}\left\{r\int_r^\infty dR\,\frac{dJ_b(R)/dR}{\Omega^2 - \omega_\beta^2}\left(1 + \frac{18\,\omega_\beta^2}{\Omega^2 - 4\,\omega_\beta^2}\right)\frac{\partial}{\partial r}\phi\right\} \qquad (37)$$

and the corresponding eigenfunction for n = 2 becomes

$$\delta\phi_2(r) = \int_r^\infty dR\,A_0(1 - 4r^2/R^2 + 3r^4/R^4)\,dJ_b(R)/dR \qquad (38)$$

Obviously, if the beam current $J_b(R)$ is a step function, then the above derived results for the rounded beam go back to that for the flat-topped beam case.

B. Dispersion relation

The derived eigenvalue equation (23) along with the perturbed beam current (35) or (37) constitute the main result for axisymmetric perturbations

which can be summarized in the general form

$$\frac{1}{r}\frac{d}{dr}\left[r\frac{d}{dr}\delta\phi(r)\ \Gamma_j(r)\right] + \frac{4\pi}{c^2}\sigma(r)\omega i\delta\phi(r) = 0 \tag{39}$$

where j = 1 or 2 representing sausage and hollowing mode respectively, so that the function $\Gamma_j(r)$ are defined by

$$\Gamma_1(r) = 1 + \frac{4\pi e\beta}{\gamma mc}\int_r^\infty dR\ \frac{dJ_b(R)/dR}{\Omega^2 - \omega_\beta^2(R)} \tag{40}$$

and

$$\Gamma_2(r) = 1 + \frac{4\pi e\beta}{\gamma mc}\int_r^\infty dR\ \frac{dJ_b(R)/dR}{\Omega^2 - \omega_\beta^2(R)}\left(1 + \frac{18\omega_\beta^2(R)}{\Omega^2 - 4\omega_\beta^2(R)}\right) \tag{41}$$

It is worth while to point out that the eigenvalue problem represented by Eq. (39) is independent of $\sigma(0)$, $J_b(0)$ and β which enables us to use them as a normalization factor for ω and Ω later in expressing the dispersion relationship. Therefore, the dispersion relation can be expressed quite generally as a functional relationship between $\Omega^2/\omega_{pb}^2\beta^2$ and $\omega\tau_d$ where the magnetic decay time for the perturbed current is defined by $\tau_d \equiv \pi\sigma(0)R_b^2/2c^2$. For any rounded beam, Eq. (39) along with (40) or (41) can be used to investigate the influence of the magnetic decay time and the plasma return current on axisymmetric instabilities.

Ironically, Eq. (39) is a standard eigenvalue problem which can be solved numerically. However, the method we adapted here enables us to

study certain specific cases which exhibit explicitly more physics. The dispersion relation that determines the complex eigenfrequency ω can be obtained easily by multiplying Eq. (39) by $r\,\delta\phi(r)$ on both sides and integrating over r from 0 to ∞. This operation gives the following result

$$\int_0^\infty dr\; r\left[d\delta\phi(r)/dr\right]^2 \Gamma_j(r) = \frac{4\pi\omega i}{c^2}\int_0^\infty dr\; r\,\sigma(r)\left[\delta\phi(r)\right]^2 \qquad (42)$$

The dependence of stability properties on the form of the conductivity profile is of considerable interest. Since the right hand side of Eq. (42) is not a function of Ω, the electrical conductivity $\sigma(r)$ only serves as a weighted function in determining the value of ω. In other words, the results become free of restriction to beams propagating in a medium with any fixed conductivity profile. For any growing wave, broadening the conductivity channel ($R_p > R_b$) will reduce ω and has a stabilizing effect. A narrow profile for $\sigma(r)$ ($R_p < R_b$) can substantially enhance the growth rate. However, the equilibrium conductivity $\sigma(r)$ in reality is a response to beam current and ambient plasma according to experimental condition and must be allowed to change with respect to time and space. We will examine this important property in the near future; Eq. (42) can be solved numerically to determine the stability properties for various system parameters of our interest. However, if the beam current is a step function as in the flat-topped beam case, Eq. (42) could lead to the following analytical results. Substituting Eqs. (36) and (40) into Eq. (42), the dispersion

relation for the m = 1 (sausage mode) becomes the simple form

$$\frac{4}{3}\, i\omega\tau_d = \frac{\Omega^2 - \omega_{pb}^2\beta_b^2\,(1 - 2f)}{\Omega^2 - 2\,\omega_{pb}^2\beta_b^2\,(1 - f)} \tag{43}$$

Similarly, by use of Eqs. (38), (41) and (42), the dispersion relation for the n = 2 (hollowing mode) becomes

$$\frac{4}{15}\, i\omega\tau_d = 1 + \frac{\omega_{pb}^2\beta_b^2}{\Omega^2 - 2\,\omega_{pb}^2\beta_b^2\,(1 - f)}\left[1 + \frac{9\,\omega_{pb}^2\beta_b^2\,(1 - f)}{\Omega^2 - 8\,\omega_{pb}^2\beta_b^2\,(1 - f)}\right] \tag{44}$$

Since the right hand side of Eqs. (43) and (44) are real always, we can expect Re (ω) = 0 all the time. So the instabilities for the flat-topped beam are purely growing modes.

C. Numerical results

In the dispersion relations (42), we fix the real frequency Ω and solve for the complex ω numerically for various system parameters to determine the wave properties. The radial dependence of the equilibrium beam current, steady plasma current and conductivity of plasma channel are all assumed to have the similar Bennett profile, but different radii are allowed in general to express the complexity of the nature. In the following, the sausage and hollowing modes will be investigated separately for various system parameters such as f, R_b and R_p. The dispersion relation will be expressed as a functional relationship between $\Omega^2/\omega_{pb}^2\beta_b^2$ and $\omega\tau_d$. The results between rounded and flat-topped beams will be compared with physical interpretation.

1. Sausage mode (n = 1)

Let us start considering the n = 1 sausage mode in the simplest case where $R_p = R_b$; i.e., the beam and plasma return currents have the same Bennett profiles of equal radii so that $f = J_p(r)/J_b(r)$ is constant everywhere for any radius r. According to Eq. (36), if the beam current $J_b(R)$ has the Bennett profile as expressed in Eq. (1), then $\delta\phi_1(r)$ can be integrated easily to obtain

$$\delta\phi_1(r) = \frac{r^2}{R_b^2}\left\{ (1 + R_b^2/r^2)/2 - \ln(1 + R_b^2/r^2) - 0.5/ (1+R_b^2/r^2) \right\} \quad (45)$$

which has the peak value at r = 0 and decreases monotonically to zero at $r = \infty$. Furthermore, the eigenfunction $\delta\phi_1(r)$ and its first derivative with respect to r (i.e., $\partial\phi_1/\partial r$) are independent of Ω and f, so that the LHS of dispersion relation (42) decides the stability criteria (stable or unstable) and the RHS determines the strength of the instability. Using Eqs. (1) and (11), Eq. (40) can be integrated to give the following analytical form

$$\Gamma_1(r) = 1 - \left\{ \frac{1}{1 + \frac{r^2}{R_b^2}} + \frac{\Omega^2}{\omega_{pb}^2\beta_b^2 2(1-f)} \ln\left[1 - \frac{2(1-f)\omega_{pb}^2\delta_b^2}{(1+\frac{r^2}{R_b^2})\ \Omega^2}\right]\right\}(1-f)^{-1} \quad (46)$$

Note that $\Gamma_1(r)$ is complex with the definition for the complex logarithm

$$\ln Z \equiv \ln r + i\theta \quad (47)$$

where $z \equiv x + iy$ and $r = (x^2 + y^2)^{1/2}$, $\theta = \tan^{-1}(y/x)$. It becomes apparent that the intrinsic singularity appears in Eq. (30) has been replaced by the logarithmic singularity as explicitly shown in Eq. (46) as we mentioned

before; for any fixed Ω and f, the pole for logarithmic singularity can be located from the limit $\lim_{z\to 0} \ell n(z)$ which gives

$$R_S^2 = R_b^2 \left[\frac{2(1 - f)\omega_{pb}^2 \beta_b^2}{\Omega^2} - 1 \right] \tag{48}$$

It is because $\delta\phi_1(r)$ obtained in (45) is a strong monotone decreasing function, with respect to increasing r, the integrant in the LHS of Eq. (42) is almost zero near the logarithmic singularity R_s. In this regard, the perturbation is contributed essentially from the integration interval between 0 and R_s. Otherwise the LHS of Eq. (42) could approach infinity which gives the unbounded growth rate.

The results of solving Eqs. (42) and (43) give the unstable regions as shown in Fig. 1 for different values of f and Ω. The dashed and solid lines are for the flat-topped and rounded beams respectively. As Eq. (43) indicated, the unstable region for the flat-topped beam is bounded by two straight lines in the f - Ω space. The value of f is restricted but taken from -1 to 1 which covers completely the possible magnitude and direction of the plasma return current in our case. The fact is for a single pulse electron beam, the plasma return current is known to be flowing in the direction opposite to the beam current. However, the situation is not always so simple. For example, as in the case where the beam is a continuous pulse train, the intermission between the pulse can cause the plasma return current going in the opposite direction before the second pulse arrives. Anyway, the unstable region for the rounded beam has been greatly reduced towards smaller Ω in the upper half of f space. It is interesting to observe that the instability exists even when $\Omega = 0$ for both beams. For $\Omega = 0$, Eq. (46) can be simplified to give

$$\Gamma_1(r) = 1 - (1 + r^2/R_b^2)^{-1} (1 - f)^{-1} \tag{49}$$

The real frequency $Re(\omega) = 0$ for the rounded beam also indicating that the perturbations are purely growing modes, which can only be driven unstable by certain amount of plasma return current, i.e., $f \neq 0$. As f increases, the rounded beam becomes unstable first at $f = 0.2$ approximately while the flat-topped beam remains stable until about $f = 0.5$. The growth rates $Im(\omega\tau_d)$ for both beams are plotted against f in Figure 2 when $\Omega = 0$. The growth rates are approaching infinity in the limit of $f = 1$ as one can expect. Because the plasma return current cancels the beam current completely and the self-magnetic pinched force no longer exists.

If $\Omega \neq 0$, the growth rates versus Ω^2 for the flat-topped beam are shown in Figure 3 for various values of fractional current neutralization f. The growth rates could go to infinity no matter what value of f is chosen because of the singularities which appear explicitly in Eq. (43). Again, the results of $Re(\omega)$ are always zero indicating that the perturbation are purely growing modes. As to the results for rounded beam, the $Im(\omega\tau_d)$ and $Re(\omega\tau_d)$ for various f are shown versus Ω^2 in Figure 4(a) and (b) respectively. The growth rate is very small when $f = 0$ where the sausage mode is driven by magnetic decay force alone. For larger f, the growth rate increases dramatically which indicates the strong influence of the plasma return current on the instability. In comparison, the rounded beam does not have the feature of unbounded linear growth rate as in the case for the flat-topped beam. This is an important quantity for the rounded beam which is in favor of the beam propagation. As we know, if the beam is rounded, then the betatron frequency for each electron is not unique. A wave with a given real frequency Ω is resonant with portion of the beam electrons only, but not

all of them, and the resonant electrons tend to be localized in particular radial ranges of the beam; the oscillation frequency $Re(\omega)$ as shown in Figure 4(b) increases linearly with respect to Ω^2. The reason of being that is very simple. As one can see in Eq. (42) the $Re(\omega)$ comes from $Im(\Gamma_1(r))$, and the imaginary part of $\Gamma_1(r)$ is contributed only from the pole at $\Omega = \omega_\beta$ according to Eq. (40) if the path of integration is chosen along the Re(R) axis. By Cauchy's theorem a contour can be deformed without crossing the singularity and then applying the theorem of residues for evaluating the definite integral in Eq. (40), which gives eventually the same unique value of πi. More specifically, the last term in Eq. (46) has a logarithmic singularity from which a value of πi is obtained according to Eq. (47). Clearly, the term is linearly proportional to Ω^2.

The electrical conductivity of the plasma channel is a rather complicated quantity characterized by a radial profile $\sigma(r)$ which determines the radial distribution of the plasma return current. For simplicity, the electrical conductivity $\sigma(r)$ and the plasma return current $J_p(r)$ are assumed to be steady and have the Bennett profiles of equal radii; usually the plasma return current flows at larger radius than the beam current at lower pressure because electric breakdown considerably spreads the conductivity channel. On the contrary, the higher pressure forces the plasma return current concentrating towards the beam axis. Therefore, without loss of generality, it is our interest to consider these two extreme cases where $R_p \neq R_b$, i.e., the plasma return current $J_p(r)$ and beam current $J_b(r)$ have the same Bennett profiles but different radii. When we do this, it is important to remember that the

restriction on fractional current neutralization f as shown in Eq. (13) has to be enforced so that the equilibrium beam profile may exist. Furthermore, under the condition of $R_p \neq R_b$, it is more convenient to use the effective current neutralization f_{eff} as defined in Eq. (5) instead of f.

First, let us consider the case of $R_p > R_b$. Figure (5) demonstrates the change of unstable region in the Ω - f_{eff} space due to different ratio of R_p/R_b. As $f_{eff} = 0$, the unstable regions in Ω domain are identical because there is no plasma return current so that the ratio of R_p/R_b is irrelevant. The electrical conductivity $\sigma(r)$ serves as a weighting function in determining the growth rate of instability. For $f_{eff} \neq 0$, the instability growth region shrinks in the Ω space but extends towards higher negative f_{eff} region as the ratio of R_p/R_b increases. If $f_{eff} < 0$, the expanded plasma return current flows in the same direction as the beam current does, which is contrary to the concept used in the center-core transmission line where both currents flow in the directions opposite to each other. No wonder it is more unstable for larger ratio of R_p/R_b; as far as the growth rate is concerned, Figure (6) shows the solution $(\omega\tau_d)$ versus Ω^2 for various f_{eff} when $R_p = 2\ R_b$. The growth rates $Im(\omega\tau_d)$ increases as f_{eff} increases. Obviously, the growth rates and the magnetic decay force $Re(\omega\tau_d)$ are smaller when comparing to those in Figure (4) where $R_p = R_b$, which indicates that the increase of plasma current radius aids stability for $f_{eff} > 1$.

Now let us consider the other extreme case where $R_p < R_b$, the results for the unstable regions in Ω - f_{eff} space are shown in Figure (7) for different ratio of R_p/R_b. The current neutralization f or effective current neutralization f_{eff} has to be restricted according to Eq. (14) as a minimum requirement for the radial confinement of the Bennett

beam. As a result, there is a forbidden region for each case in Figure (7) which fulfills the inequality $f_{eff} < (R_p/R_b)^2$ in f_{eff} domain; e.g., $f_{eff} > .25$ when $R_p = 0.5\ R_b$.

As the plasma channel is narrower than the beam current, the unstable region increases in Ω space for $f_{eff} > 0$ but remains very stable for $f_{eff} < 0$. As $f_{eff} < 0$, the self-magnetic pinched force has been enhanced somewhat by the plasma return current which flows in the same direction as the beam current so that the beam is very stable. The growth rates for $R_p = 0.5\ R_b$ are shown in Figure (8) versus Ω^2 for different f_{eff}. The value of f_{eff} is chosen only from 0 to 0.2 which corresponds that f increases from 0 to 0.8 because of the restriction of Eq. (14). The growth rate can be very large even for small value of f_{eff}. Finally, let us summarize the sausage mode calculations by presenting the criteria for non-oscillatory growth region in the f_{eff} - R_p/R_b space which is shown in Figure (9). It is a purely growing mode where $\Omega = 0$ and $Re(\omega) = 0$. As one can see, the sausage mode of this kind can only be excited when $f_{eff} > 0$.

2. Hollowing mode

Next to the sausage mode, we want to consider and therefore do the similar calculations for the hollowing mode (n = 2). For the simplest case where $R_p = R_b$, the eigenfunction (38) has the form after integration

$$\delta\phi_2(r) = \delta\phi_1(r) - 1.5(r/R_b)^4 \left\{0.75 + 0.25\ X^2 - 1.5\ X + 1.5\ \ln X + 0.5/X\right\} \tag{50}$$

where $\delta\phi_1(r)$ is equivalent to that shown in Eq. (45) and $X \equiv 1 + R_b^2/r^2$ for simplification. $\delta\phi_2(r)$ is also a monotone decreasing function which vanishes as $r \to \infty$. Likewise the expression for $\Gamma_2(r)$ in Eq. (41) can be integrated to give

$$\Gamma_2(r) = \Gamma_1(r) + \frac{9}{4} \frac{\Omega^2}{\omega_{pb}^2\beta_b^2(1-f)^2}\left\{\frac{\omega_{pb}^2\beta_b^2(1-f)}{2\Omega^2} - \frac{5}{16}\ln X + \frac{1}{3}\ln\left[X - \frac{2\omega_{pb}^2\beta_b^2(1-f)}{\Omega^2}\right] - \frac{1}{48}\ln\left[X - \frac{8\omega_{pb}^2\beta_b^2(1-f)}{\Omega^2}\right]\right\} \quad (51)$$

where $\Gamma_1(r)$ denotes the same expression as in Eq. (46) and $X = 1 + (R_b/r)^2$ also for simplification. As one can see in Eq. (51), the last two terms contain two logarithmic singularities which have been formed due to the two intrinsic singularities in Eq. (41). Substituting Eqs. (50) and (51) into Eq. (42), we solve the dispersion relation numerically for various system parameters. The results for the unstable regions in the Ω - f space are illustrated in Fig. (10) for the flat-topped (dashed line) and rounded beam (solid line) respectively. Note that the unstable region for the flat-topped beam is greatly reduced by the influence of the rounded beam profile. From Eq. (44) the growth rates for the flat-topped beam can be obtained easily and shown in Fig. (11) for various value of current neutralization f. Correspondingly, the $\mathrm{Im}(\omega\tau_d)$ and $\mathrm{Re}(\omega\tau_d)$ for the rounded beam are plotted against Ω^2 for various f in Fig. (12). As one can immediately see, the unbounded linear growth rates of the flat-topped beam are replaced by the finite growth rates of the rounded beam. For the rounded beam, both $\mathrm{Im}(\omega\tau_d)$ and $\mathrm{Re}(\omega\tau_d)$ increases as f increases. Note that the growth rate is very large even when f = 0, the hollowing mode is driven unstable by the magnetic

decay force along. It is further noticed that the peaks of the growth rates can be found near the dashed line as shown in Fig. (10) where the growth rates for the flat-topped beam become infinity.

Now, we are ready to make a comparison between the sausage and hollowing mode perturbations for the rounded beam. The growth rates as shown in Fig. (12) for the hollowing mode are generally larger than that of the sausage mode in Fig. (4). Fow example, when f = 0, the growth rate for the hollowing mode is at least an order of 2 larger than the n = 1 sausage mode. It concludes that the magnetic decay force plays an important role in exciting the hollowing mode. As f increases, the ratio of the growth rate between the two modes reduces gradually but still remains a factor of 10 approximately when f = 0.8. As $f < 0$, the plasma return current has the stabilizing effect on both modes, because it introduces additional self-magnetic pinched force for the beam. The sausage modes are very stable but not for the hollowing modes because the growth rates are very large even when f = 0, it certainly needs more plasma return current flowing in the same direction to stabilize the beam. Generally speaking, because of the huge growth rate of the hollowing mode, it seems unlikely to have any sausage mode oscillations or enough time for them to grow before the hollowing mode totally destroys the beam. Now, if one looks closely in Figs. (4) and (12) again, one can find another big difference between the results for the sausage and hollowing modes. Namely the maximum growth rate for various f occurs near small value of Ω for the sausage mode but span to very large values of Ω except for those with high current neutralization for the hollowing mode. Recall that the perturbation we are interested is in the low frequency regime. The theory derived here is not necessarily correct for high frequency perturbation. The beam electrons at various energy level oscillate with various betatron frequency at different radius. From Eq. (11), the betatron frequency $\omega_\beta(r)$ has the maximum value $\omega_\beta(0)$ at the beam axis and

decreases outwards outwards radially. Because of the natural oscillation of the electrons, it is likely that the waves are excited primarily in the frequency range of $0 < \Omega < \omega_\beta(0)$. In this respect, although the growth rates of the hollowing mode are very large in general, one has to be very careful about the location of Ω where the peaks of growth rates occur. One could argue that it is almost impossible to have waves excited with very large frequency Ω (e.g. $\Omega > \omega_\beta(0)$) unless the perturbation is imposed externally. In Fig. (12) the maximum growth rate occurs near the region where $\Omega > \omega_\beta(0)$ which is not likely to happen in the nature. Nevertheless, the maximum growth rate for $f > 0.5$ can be found in the region of Ω satisfying $\Omega < \omega_\beta(0)$. It indicates the possible excitation of the hollowing mode naturally when the current neutralization is high. There has been some evidence from numerical simulation results.[8] For example, there is no sausage mode oscillation which has even been observed experimentally for a self-pinched electron beam propagating in the plasma. In addition, numerical simulation has indicated that the electron beam becomes hollow if the current neutralization exceeds 0.5 or so.

It is straight forward to extend the calculation of hollowing mode to consider the case where $R_p \neq R_b$, namely the beam and plasma return currents have the similar Bennett profiles but unequal radii. First, for the case $R_p > R_b$, Fig. (13) illustrates the various growth regions in the Ω - f_{eff} space for different ratio of R_p/R_b. The beam seems more stable as the ratio R_p/R_b increases, because the unstable region in Ω space have been greatly reduced and concentrated towards higher Ω domain. The growth rates versus Ω^2 for $R_p = 2R_b$ are shown in Fig. (14) for various f_{eff}. One can see clearly that the growth rates are not a strong function of f_{eff} any more. The reason is very simple, the hollowing mode perturbation is highly unstable at $f = 0$ where the instability is driven simply by the magnetic decay force.

The plasma return current tries to change the situation. However, under the condition of $R_p > R_b$, the amount of plasma return current overlapped with the beam remains almost unchanged even for very large ratio of R_p/R_b. On the other hand, for the second case where $R_p < R_b$, the unstable region for the hollowing mode perturbation as shown in Fig. (15) expands very much in Ω space as the ratio of R_p/R_b decreases first (e.g., $R_p = 0.5\ R_b$), but shrinks back for further decrease of R_p/R_b, a forbidden region in the f_{eff} domain is drawn in Fig. (15) where the equilibrium Bennett beam fails to exist. The growth rates for $R_p = 0.5\ R_b$ are plotted in Fig. (16) against Ω^2 for various f_{eff}. It is very clear that as f_{eff} increases the growth rate increases and can go to infinity (e.g., $f_{eff} > 0.15$ or $f > 0.6$ equivalently). For higher f_{eff}, this is a very unstable situation for the beam because of the hollowing mode oscillations. Once the self-magnetic pinched force is reduced near the axis by the presence of the plasma return current, it is not difficult to understand why the beam electrons on the beam axis can easily be expelled by the highly concentrating return current. As long as the hollowing mode exists, the beam is going to become annular eventually and expand continuously.

IV. Conclusions

The equilibrium and stability of an intense relativistic self-pinched electron beam propagating in a resistive plasma channel has been studied by the Vlasov-Maxwell Theory. For the thermal equilibrium distribution function, the steady and equilibrium electron beam without plasma return current has the familiar Bennett radial density profile. When the plasma return current is unavoidable in the system, the minimum requirement for the radial confinement of the electron beam has been derived to restrict the degree of current neutralization. An analytical theory of the axisymmetric perturbations including the sausage ($n = 1$) and hollowing ($n = 2$) modes has been derived for an electron beam with rounded radial current profile. Complete space-charge neutralization and the paraxial beam electron motion have been assumed in the derivation.

In this paper, we have considered in particular a wave with real frequency Ω and $\mathrm{Im}(\omega) > 0$ which has a certain wave amplitude at the beam head and grows spatially backward along the beam. It is essentially a convective instability. A numerical calculation has been made for the special case where the equilibrium radial distribution of the beam and plasma return current, as well as electrical conductivity of the plasma channel, have similar Bennett profiles but different radii is also allowed. The results for axisymmetric perturbations have shown that the important system parameters such as the effective current neutralization, the radial profile of electrical conductivity of plasma channel, beam and plasma return current are very sensitive in determining the stability behavior of an electron beam. First, the results for the rounded beam have been compared to that of the flat-topped beam. Generally speaking, there is no linear bound on wave growth for the flat-topped beam. For the rounded beam, the finite growth rates for the hollowing mode are much larger than that of the sausage

mode. In practice, it has been concluded that the naturally excited hollowing mode oscillation is more likely to happen when the current neutralization exceeds about 0.5.

It has been shown from the calculations the high-frequency hollowing mode perturbations (i.e., $\Omega^2/\omega_{pb}^2\ \beta_b^2 \approx 2$) can be driven unstable by the magnetic decay force alone where the phase lag between the transverse displacement of the beam and the magnetic field drives the instability. The naturally occurring plasma return current can flow either in the same or in the opposite direction as that of the beam current. The one flows in the same direction introduces additional self-magnetic pinched force which intends to stabilize the beam. On the contrary, the one in the opposite direction reduces the pinched force and thus enhances the perturbations. As $R_p < R_b$ where a narrow conducting channel confines the plasma return current, the highly concentrating return current on beam axis is very dangerous for hollowing and destroying the beam.

Finally, it is of importance to compare the growth rates of the axisymmetric modes to those of the hose instability. Generally, the growth rates for the sausage mode are much smaller than that of the hose modes as obtained from Figure 5 of Reference 2. This may well explain why the sausage mode oscillation has not been found experimentally or in numerical simulation. It is simply because of the domination of the hose mode, the beam could be expelled from its channel even before the sausage mode starts to grow. However, the maximum growth rates for the hollowing mode are larger in most cases or at least comparable to those of the hose mode which addresses very clearly the importance of the hollowing mode oscillation in the beam propagation.

V. ACKNOWLEDGEMENTS

The authors are grateful to Dr. Martin Lampe for his useful comments on this work.

This research was supported in part by the Independent Research Fund at the Naval Surface Weapons Center and in part by Defense Advanced Research Projects Agency and NAVSEA.

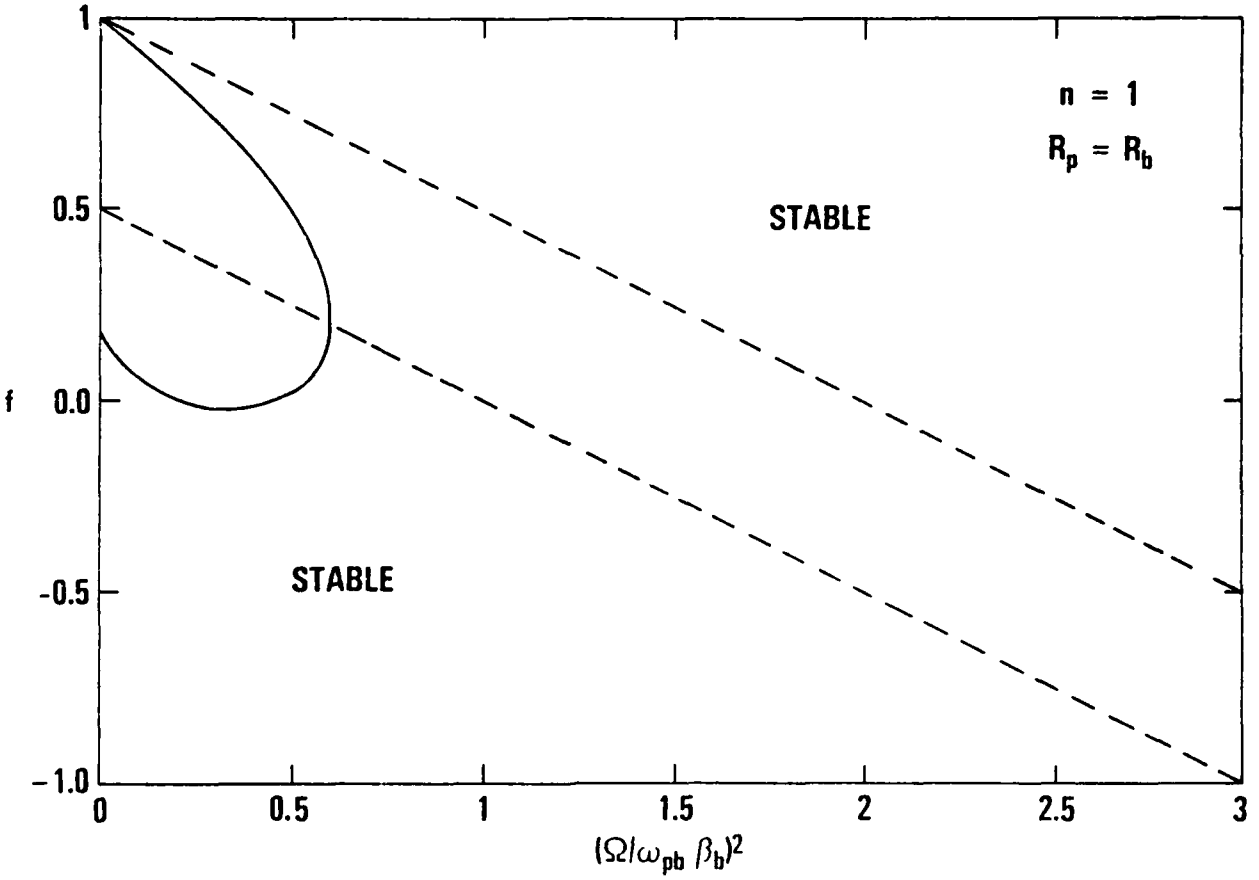

FIGURE 1. THE GROWTH REGION FOR THE SAUSAGE MODE WITH $R_p = R_b$ IN THE $f - \Omega$ SPACE (DASHED LINE FOR FLAT-TOPPED AND SOLID LINE FOR ROUNDED BEAM RESPECTIVELY)

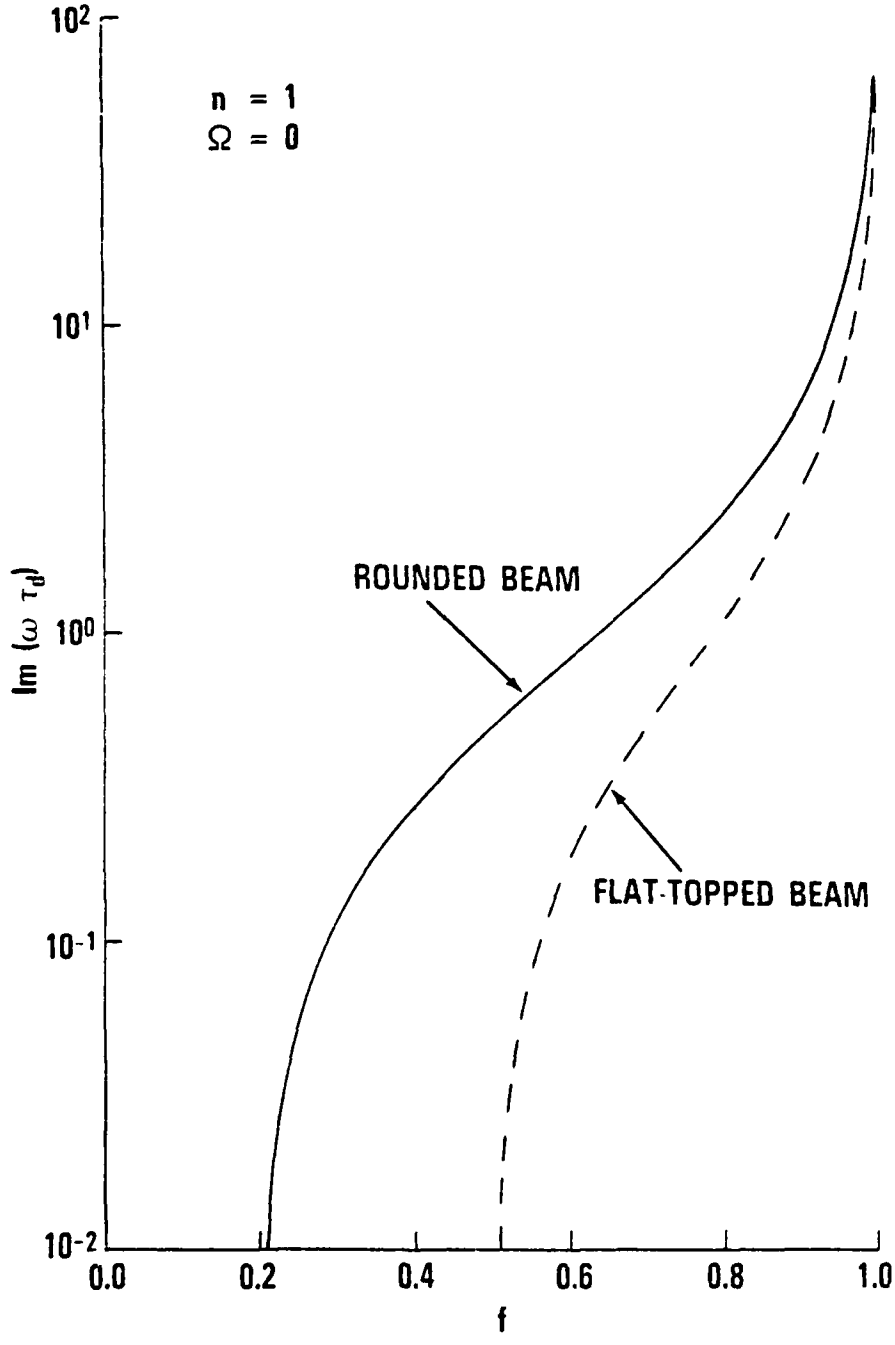

FIGURE 2. THE GROWTH RATE OF NON-OSCILLATORY SAUSAGE MODE OSCILLATION VERSUS f FOR THE ROUNDED AND FLAT-TOPPED BEAMS

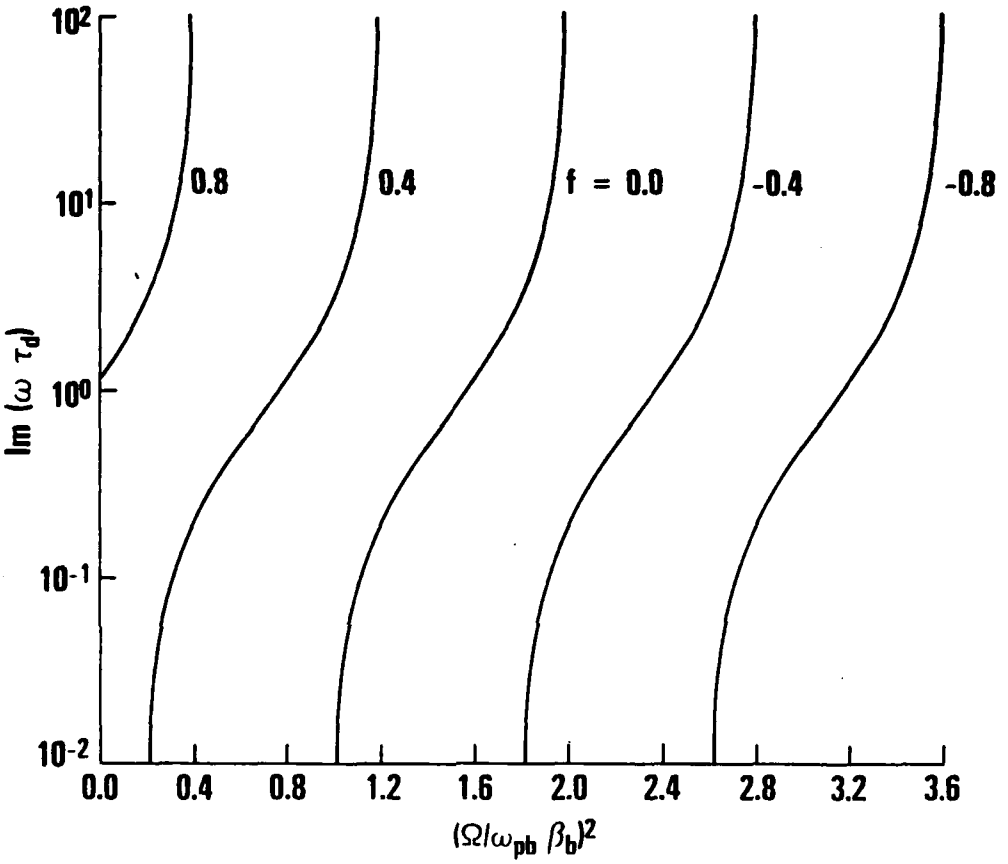

FIGURE 3. THE GROWTH RATE OF THE SAUSAGE MODE VERSUS Ω^2 FOR VARIOUS f FOR THE FLAT-TOPPED BEAM

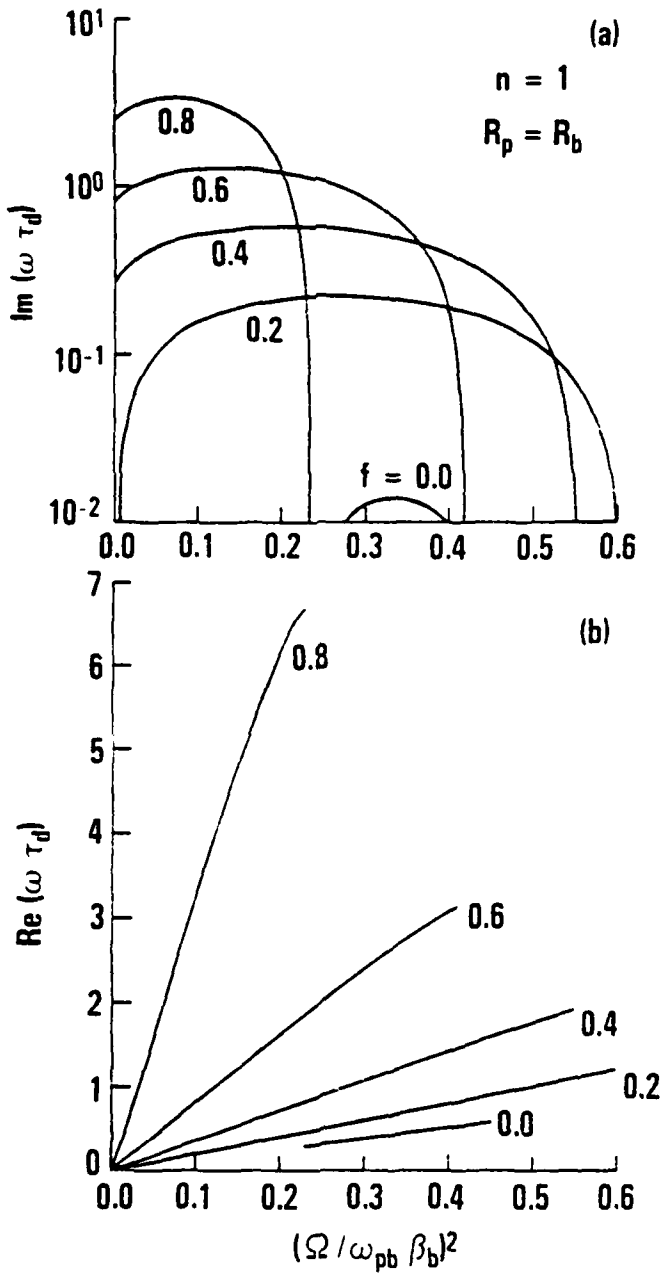

FIGURE 4. GROWTH RATE $I_m(\omega)$ AND REAL EIGENFREQUENCY $R_e(\omega)$ VERSUS Ω^2 FOR THE SAUSAGE MODE OF A BENNETT BEAM WITH $R_p = R_b$ FOR VARIOUS f

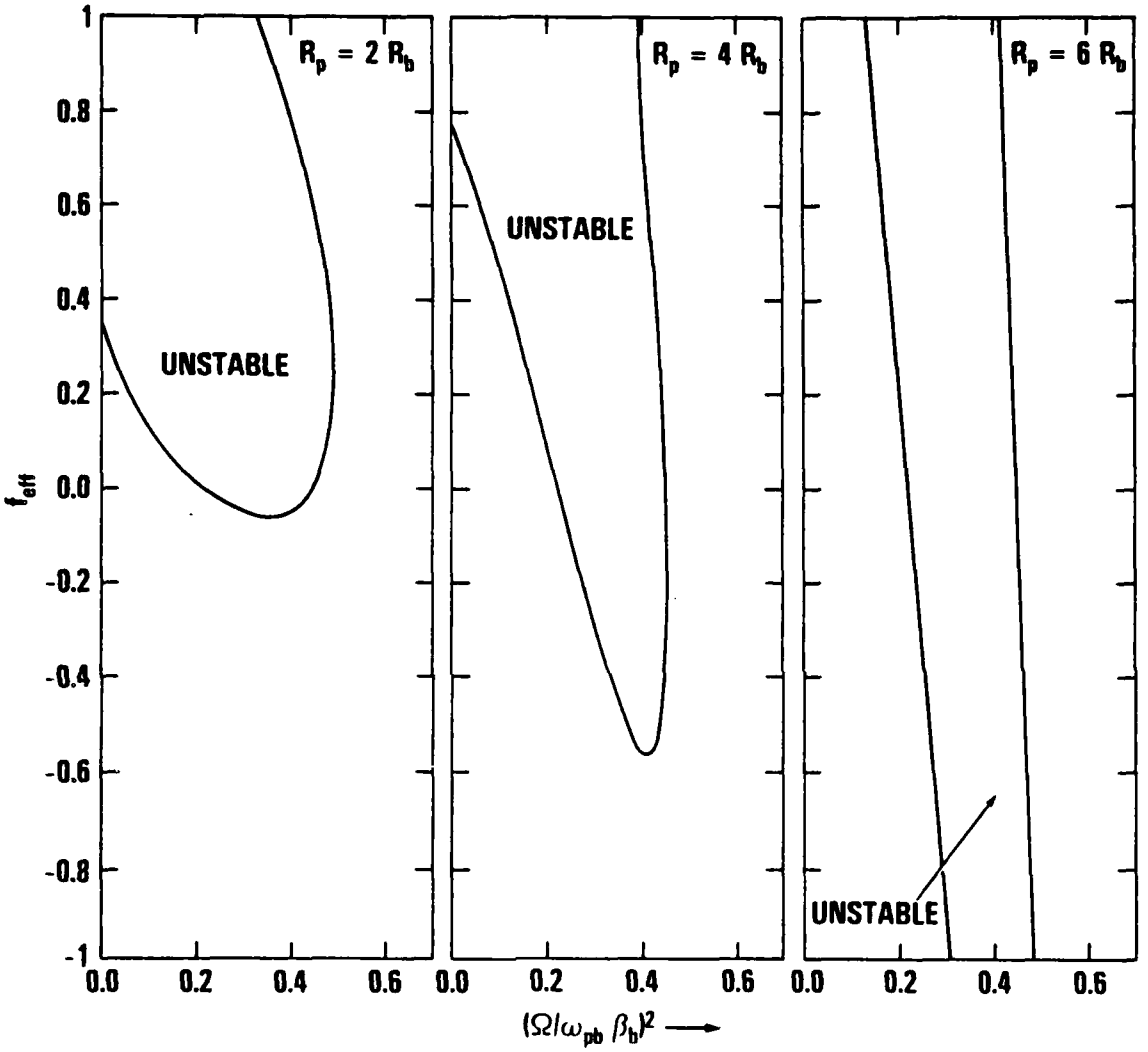

FIGURE 5. THE UNSTABLE REGION OF THE SAUSAGE MODE OF THE BENNETT BEAM IN THE f_{eff} – Ω SPACE FOR R_p/R_b = 2, 4, 6 RESPECTIVELY

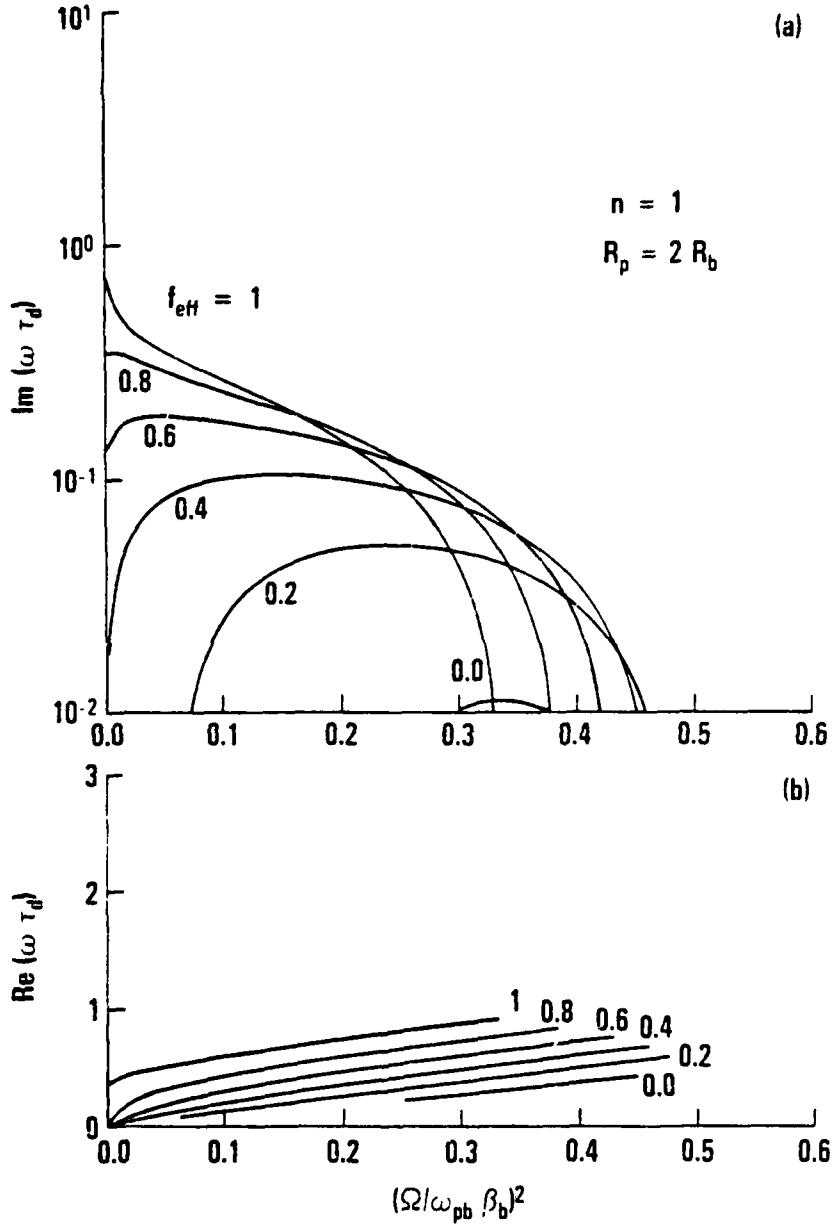

FIGURE 6. GROWTH RATE Im(ω) AND REAL EIGENFREQUENCY $R_e(\omega)$ VERSUS Ω^2 FOR THE SAUSAGE MODE OF A BENNETT BEAM WITH $R_p = 2\ R_b$ FOR VARIOUS f_{eff}

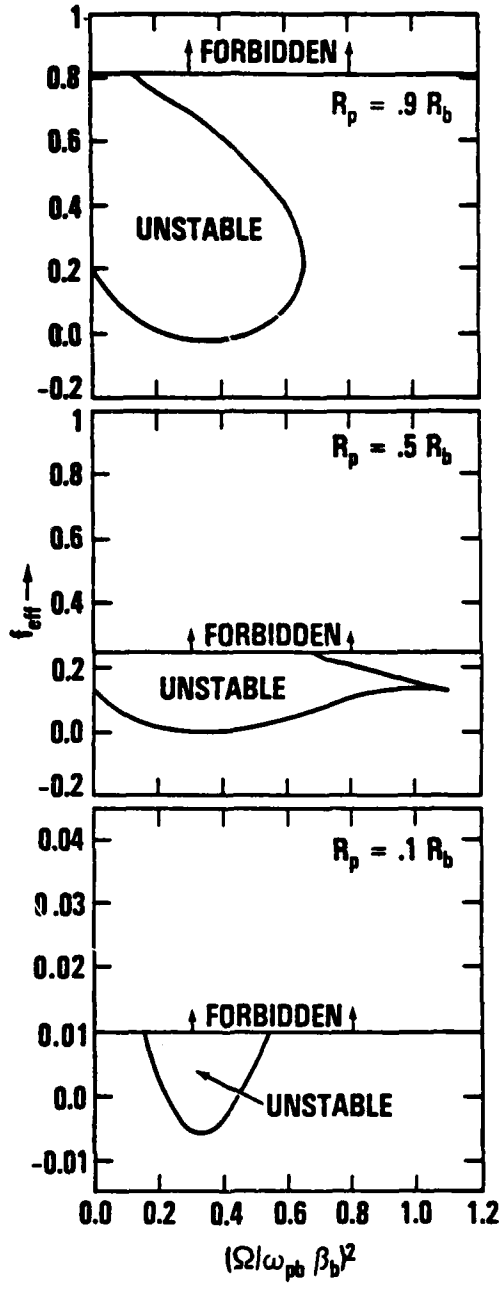

FIGURE 7. THE UNSTABLE REGION OF THE SAUSAGE MODE OF THE BENNETT BEAM IN THE $f_{eff} - \Omega$ SPACE FOR R_p/R_b = 0.9, 0.5, AND 0.1, RESPECTIVELY

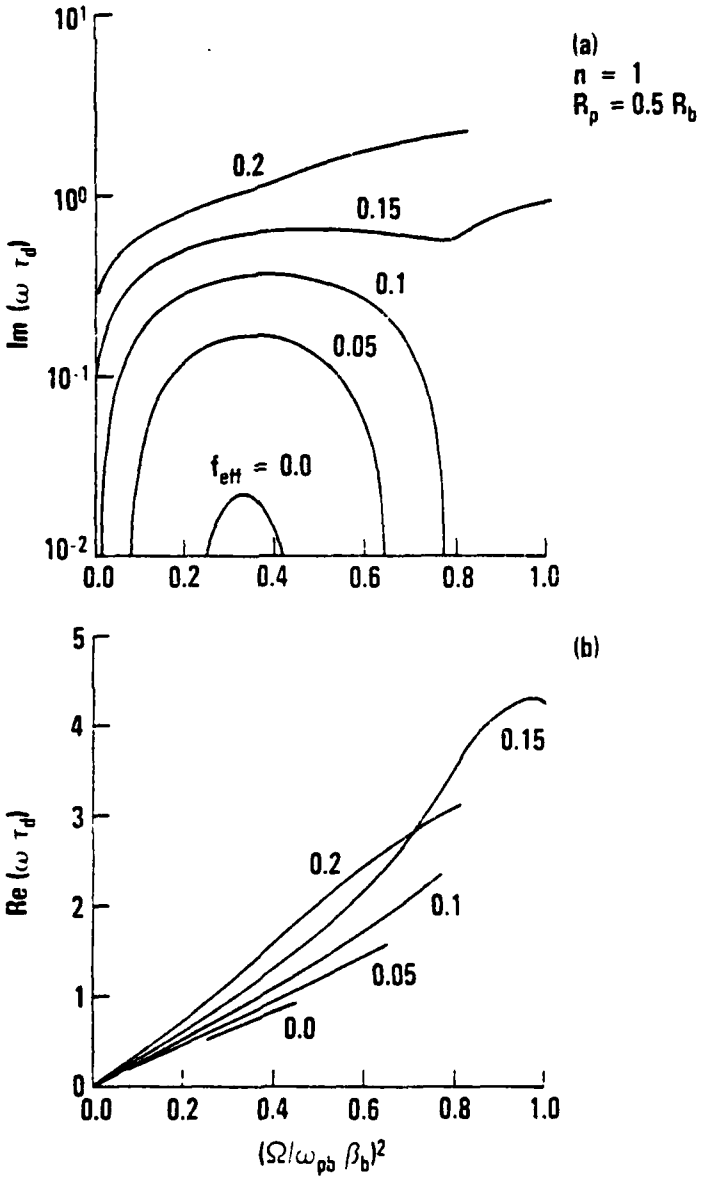

FIGURE 8. GROWTH RATE Im(ω) AND REAL EIGENFREQUENCY Re (ω) VERSUS Ω^2 FOR THE SAUSAGE MODE OF A BENNETT BEAM WITH R_p = 0.5 R_b FOR VARIOUS f_{eff}

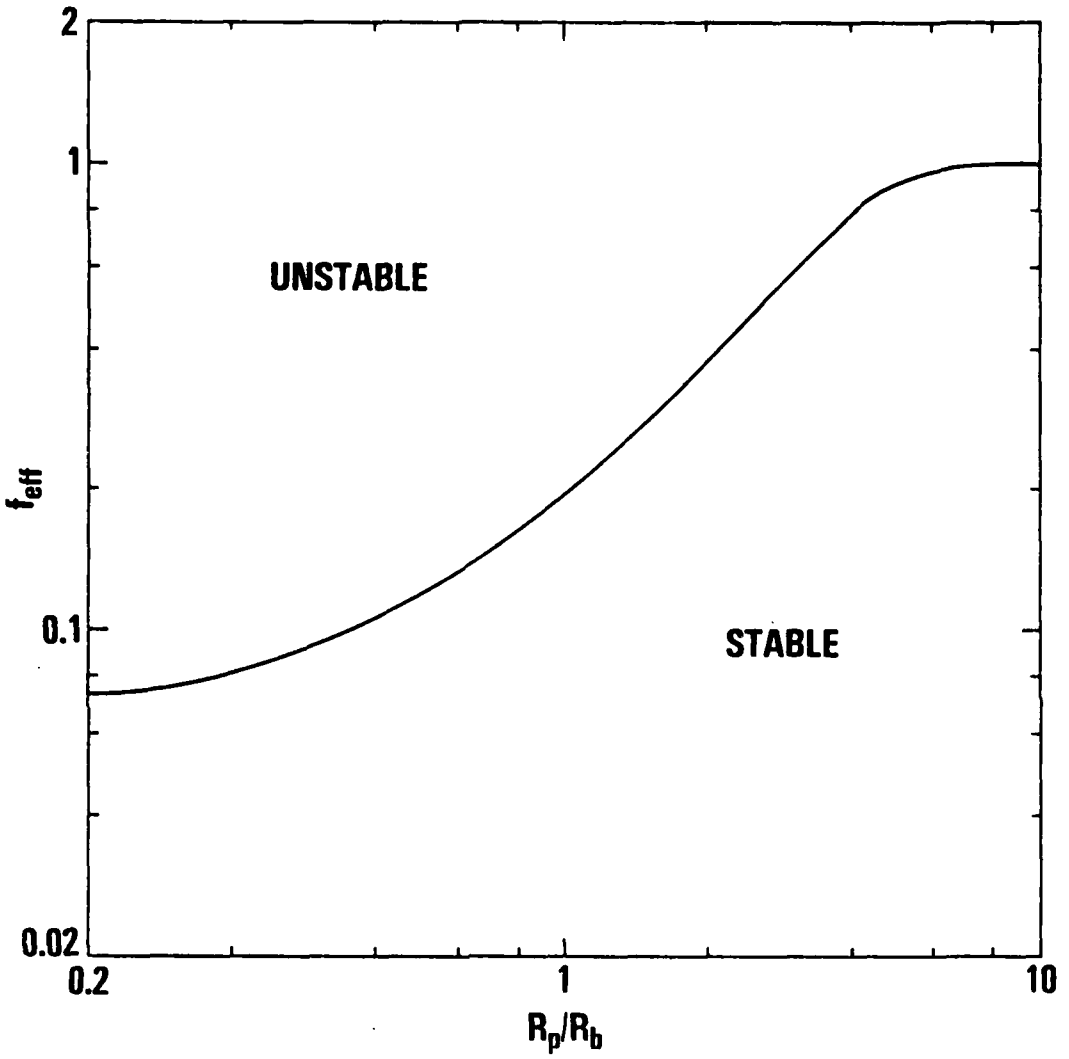

FIGURE 9. NONOSCILLATORY GROWTH REGION FOR A BENNETT BEAM IN THE $f_{eff} - R_p/R_b$ SPACE

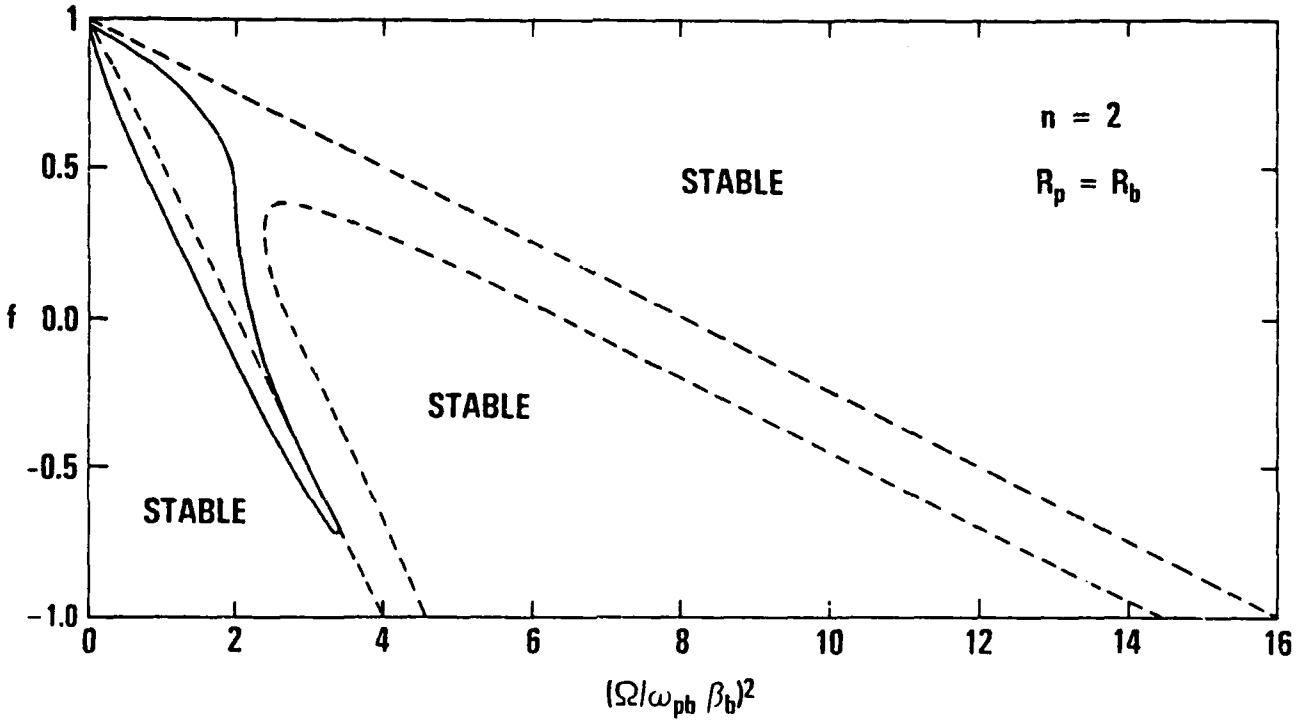

FIGURE 10. THE GROWTH REGION FOR THE HOLLOWING MODE WITH $R_p = R_b$ IN THE $f - \Omega$ SPACE (DASHED LINE FOR FLAT-TOPPED AND SOLID LINE FOR ROUNDED BEAM RESPECTIVELY)

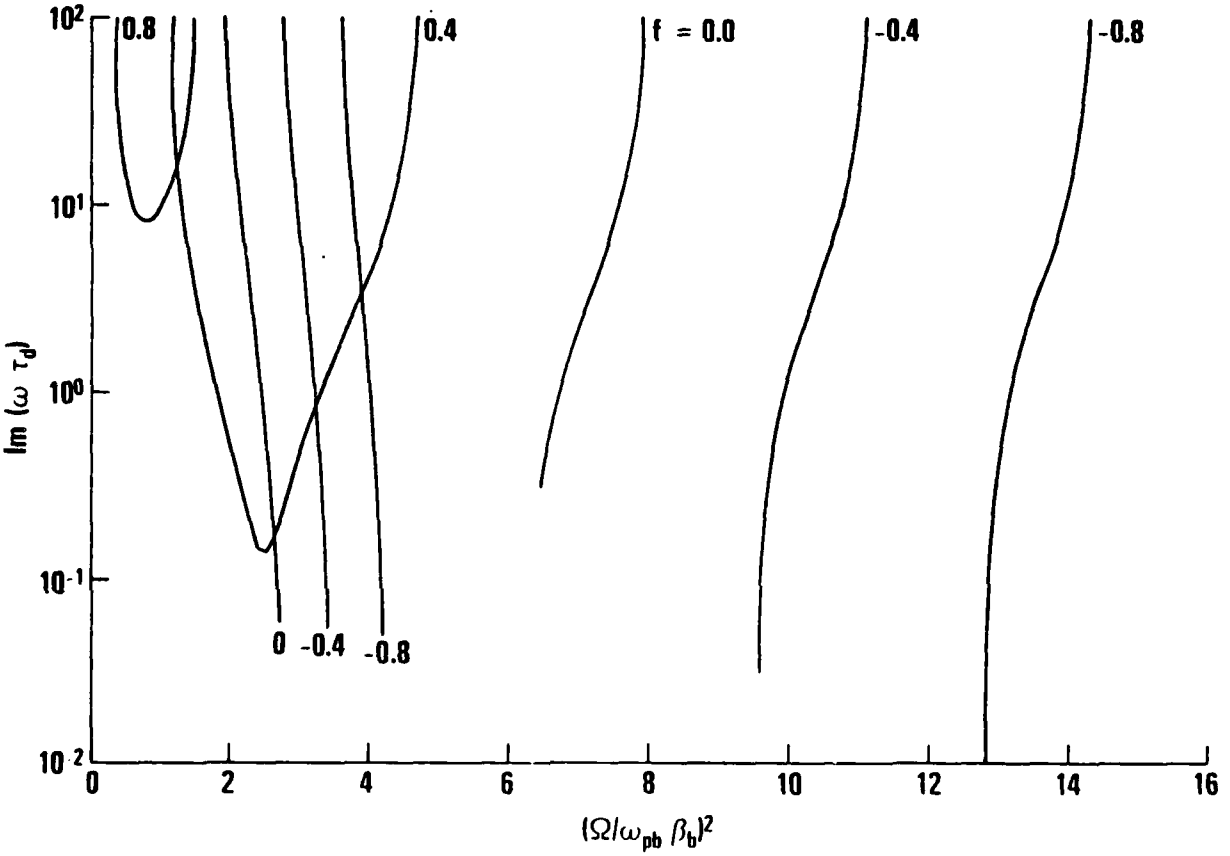

FIGURE 11. THE GROWTH RATE OF THE HOLLOWING MODE VERSUS Ω^2 FOR VARIOUS f FOR THE FLAT-TOPPED BEAM

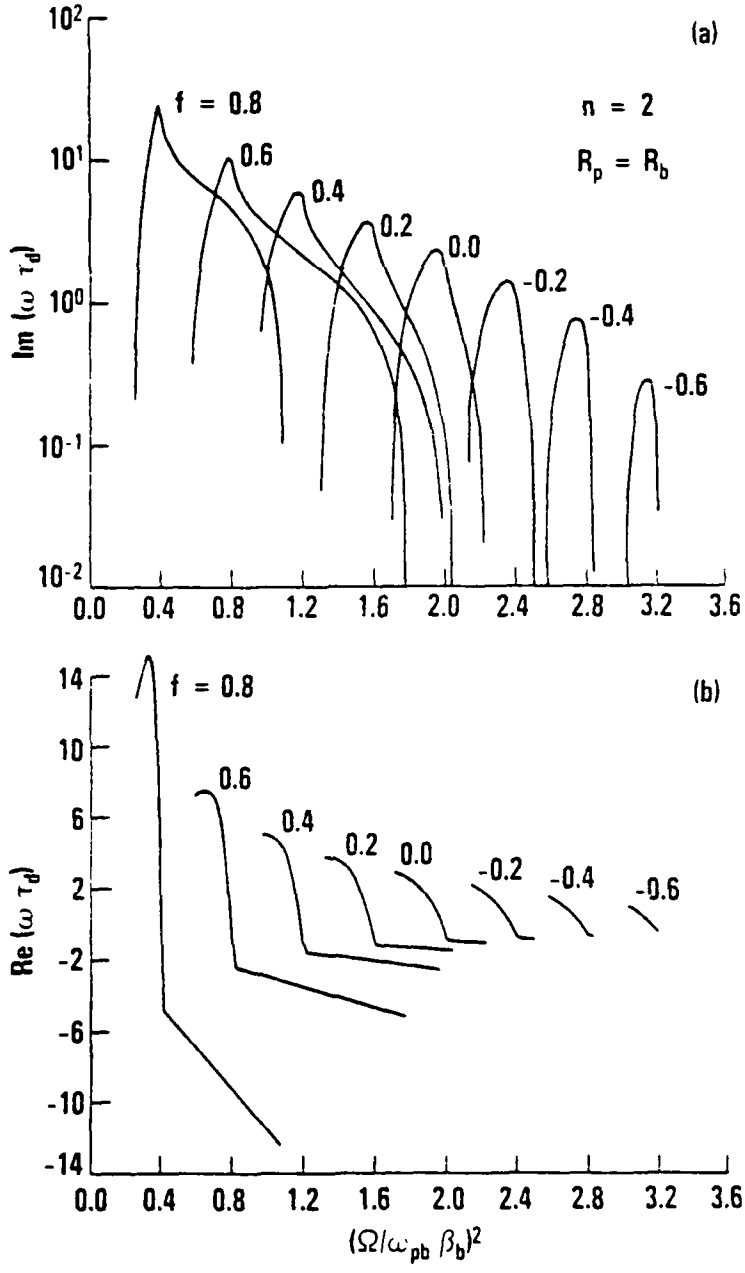

FIGURE 12. GROWTH RATE Im(ω) AND REAL EIGENFREQUENCY Re(ω) VERSUS Ω^2 FOR THE HOLLOWING MODE OF A BENNETT BEAM WITH $R_p = R_b$ FOR VARIOUS f

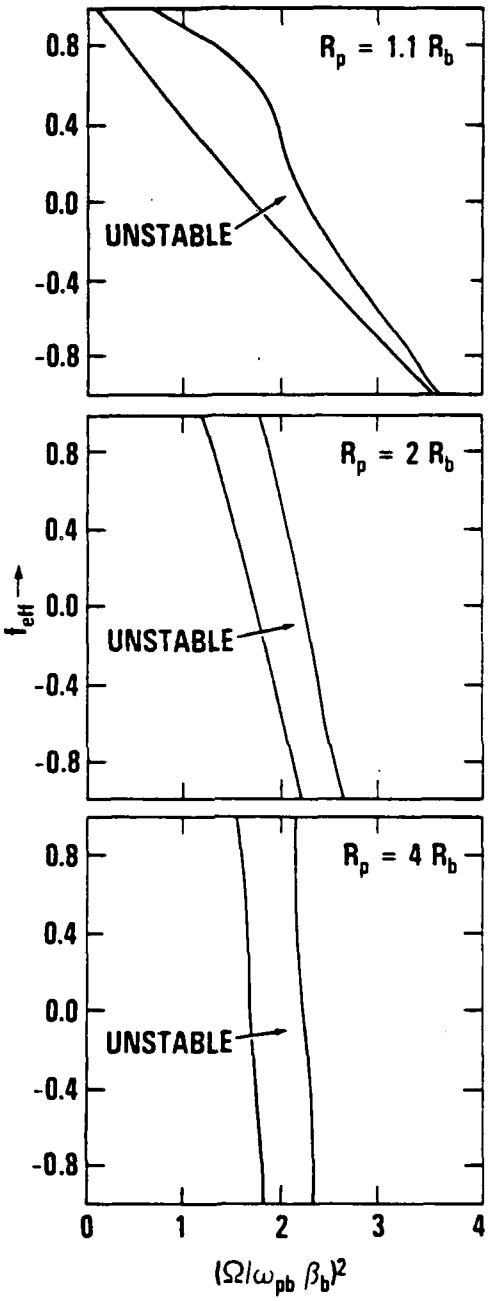

FIGURE 13. THE UNSTABLE REGION OF THE HOLLOWING MODE OF THE BENNETT BEAM IN THE $f_{eff} - \Omega$ SPACE FOR R_p/R_b = 1.1, 2, 4, RESPECTIVELY

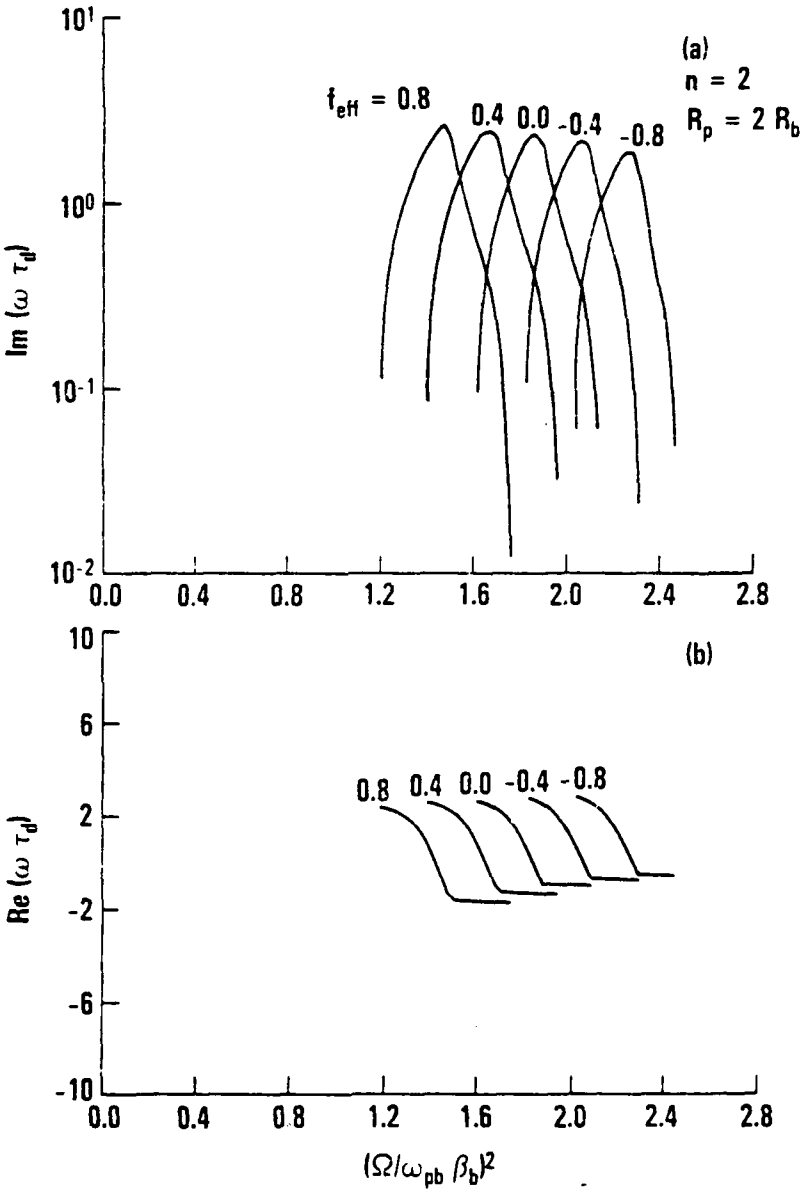

FIGURE 14. GROWTH RATE Im(ω) AND REAL EIGENFREQUENCY Re(ω) VERSUS Ω^2 FOR THE HOLLOWING MODE OF A BENNETT BEAM WITH $R_p = 2\ R_b$ FOR VARIOUS f_{eff}

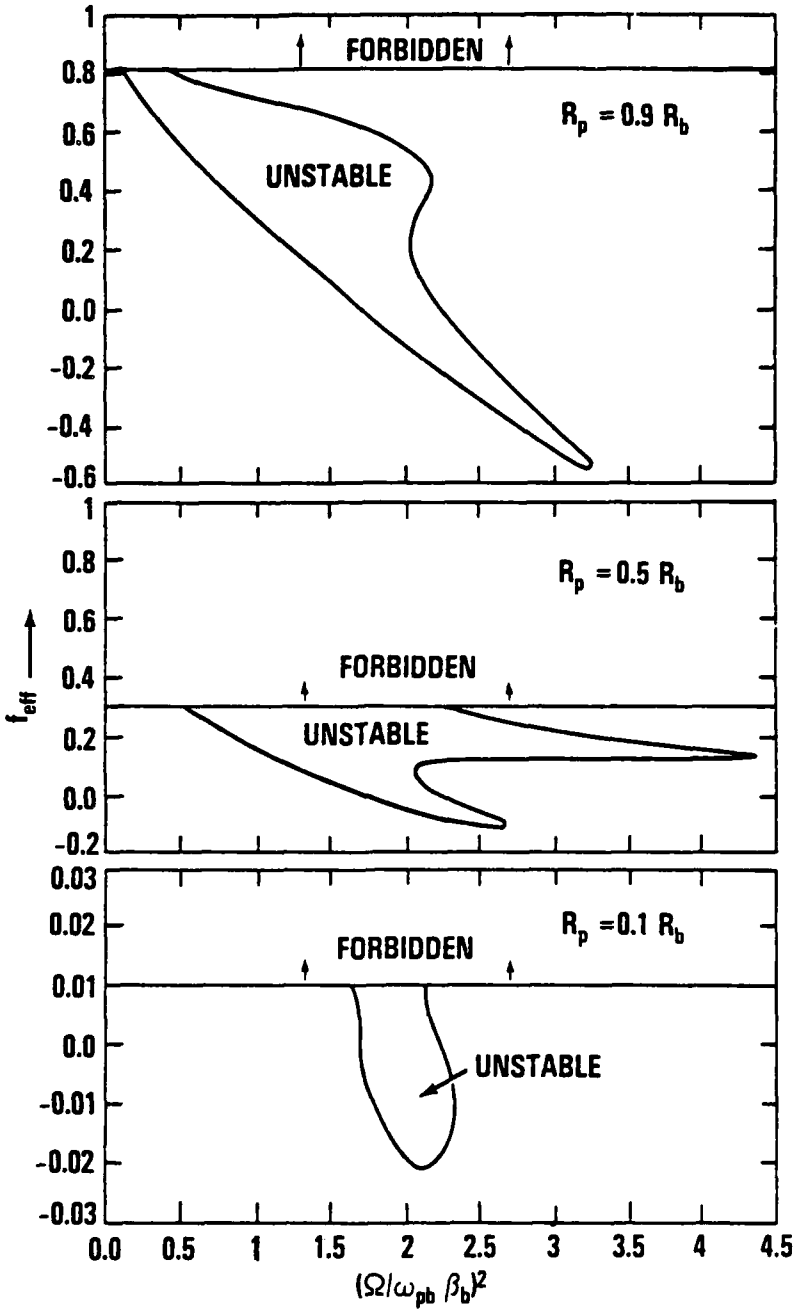

FIGURE 15. THE UNSTABLE REGION OF THE HOLLOWING MODE OF THE BENNETT BEAM IN THE $f_{eff} - \Omega$ SPACE FOR R_p/R_b = 0.9, 0.5, 0.1, RESPECTIVELY

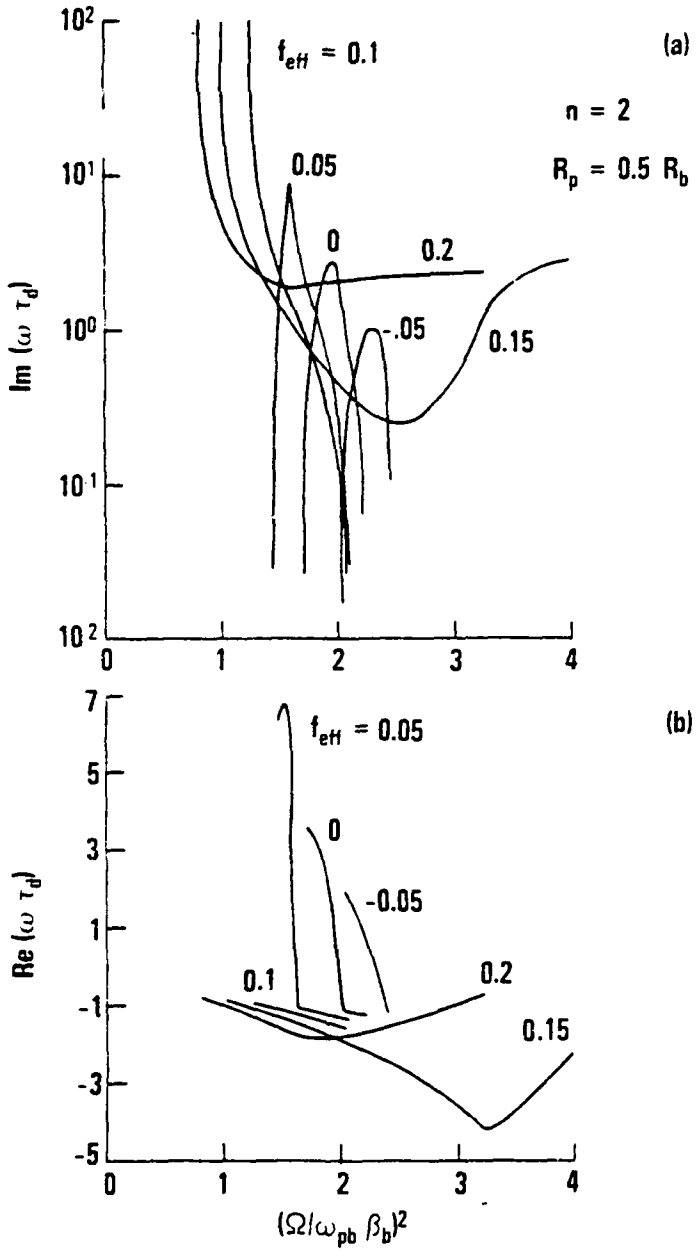

FIGURE 16. GROWTH RATE Im(ω) AND REAL EIGENFREQUENCY Re(ω) VERSUS Ω^2 FOR THE HOLLOWING MODE OF A BENNETT BEAM WITH R_p = 0.5 R_b FOR VARIOUS f_{eff}

REFERENCES

1. H. S. Uhm and M. Lampe, Phys. Fluids 23, 1574 (1980).
2. W. M. Sharp, M. Lampe and H. S. Uhm, Phys. Fluids 25, 1456 (1982).
3. E. P. Lee, Phys. Fluids 21, 1327 (1978).
4. E. J. Lauer, R. J. Briggs, T. J. Fessendon, R. E. Hexter and E. P. Lee, Phys. Fluids 21, 1344 (1978).
5. H. S. Uhm and M. Lampe, Phys. Fluids 24, 1553 (1981).
6. E. P. Lee, Lawrence Livermore National Laboratory Report UCID - 18940 (1981).
7. F. W. Chambers, Lawrence Livermore National Laboratory Report UCID - 18879 (1980).
8. M. Lampe, W. M. Sharp, G. Joyce, R. Hubbard and H. S. Uhm, Proc. of 4th International Topical Conference on High-Power Electron and Ion-Beam Research and Technology, edited by Doucet and Buzzi (Palaiseau, France, 1981, p. 165).
9. H. S. Uhm and M. Lampe, Phys. Fluids, 25, 1444 (1982).
10. W. H. Bennett, Phys. Rev. 45, 890 (1934).
11. R. C. Davidson and H. S. Uhm, Phys. Fluids 22, 1375 (1979).
12. J. D. Lawson, "The Physics of Charged-Particle Beams" (Clarendon Press, Oxford, 1977).
13. H. Alfvén and C. G. Fälthammar, "Cosmical Electrodynamics" (Oxford, U.P., 1963).

DISTRIBUTION

	Copies
Dr. Richard E. Aamodt Science Application Inc. 934 Pearl St. Suite A Boulder, CO 80302	1
Dr. Saeyoung Ahn Code 5205 Naval Research Lab. Washington, D.C. 20375	1
Dr. Wahab A. Ali Naval Research Lab. Code 4700 4555 Overlook Ave., S.W. Washington, D.C. 20375	1
Dr. Donald Arnush TRW, Plasma Physics Dept. R1/107 1 Space Park Rodondo Beach, CA 90278	1
Dr. J.M. Baird Code 4740 (B-K Dynamics) Naval Research Lab. 4555 Overlook Ave., S.W. Washington, D.C. 20375	1
Dr. William A. Barletta Lawrence Livermore National Lab. L-321 University of California Livermore, CA 94550	1
Dr. L. Barnett Code 4740 (B-K Dynamics) Naval Research Lab. 4555 Overlook Ave., S.W. Washington, D.C. 20375	1
Dr. J. Bayless DARPA Attn: DEO 1400 Wilson Blvd. Arlington, VA 22209	1
Dr. Robert Behringer ONR 1030 E. Green Pasadena, CA 91106	1
Prof. George Bekefi Bldg. 36-213, MIT 77 Massachusetts Ave. Cambridge, MA 02139	1
Dr. Gregory Benford Physics Department University of California Irvine, CA 92717	1
Dr. Jim Benford Physics International Co. 2700 Merced St. San Leandro, CA 94577	1
Dr. Kenneth D. Bergeron Plasma Theory Div. - 5241 Sandia Laboratories Albuquerque, NM 87115	1
Dr. T. Berlincourt Office of Naval Research Department of the Navy Arlington, VA 22217	1

DISTRIBUTION (Cont.)

	Copies
Dr. I. B. Bernstein Yale University Mason Laboratory 400 Temple Street New Haven, CT 06520	1
Dr. O. Book Code 4040 Naval Research Laboratory Washington, D.C. 20375	1
Dr. Jay Boris Naval Research Lab. Code 4040 4555 Overlook Ave., S.W. Washington, D.C. 20375	1
Dr. Howard E. Brandt Harry Diamond Labs 2800 Powder Mill Road Adelph, MD 20783	1
Dr. R. Briggs Lawrence Livermore Lab. P.O. Box 808 Livermore, CA 94550	1
Dr. K. Brueckner La Jolla Institute P.O. Box 1434 La Jolla, CA 92038	1
Dr. Herbert L. Buchanan Lawrence Livermore National Lab L-321 University of California Livermore, CA 94550	1
Dr. K. J. Button Massachusetts Institute of Technology Francis Bitter National Magnet Laboratory Cambridge, MA 02139	1
Dr. Neal Carron Mission Research Corp. 735 State Street Santa Barbara, CA 93102	1
Dr. Frank Chambers Lawrence Livermore National Lab. L-321 University of California Livermore, CA 94550	1
Prof. F. Chen Dept. of E. E. UCLA Los Angeles, CA 90024	1
Dr. M. Caponi TRW Advance Tech. Lab. 1 Space Park Redondo Beach, CA 90278	1
Dr. K. R. Chu Naval Research Lab. Code 4740 4555 Overlook Ave., S.W. Washington, D.C. 20375	1
Dr. Timothy Coffey Naval Research Lab. 4555 Overlook Ave., S.W. Washington, D.C. 20375	1
Dr. W. J. Condell Office of Naval Research Code 421 Department of the Navy Arlington, VA 22217	1
Dr. G. Cooperstein Naval Research Lab. Washington, D.C. 20375	1
Dr. Edward Cornet W.J. Schafer Associates, Inc. 1901 North Fort Myer Dr. Arlington, VA 22209	1

DISTRIBUTION (Cont.)

	Copies
Prof. R. Davidson Plasma Fusion Center Massachusetts Inst. of Technology Cambridge, MA 02139	1
Dr. J. Dawson Dept. of Physics UCLA Los Angeles, CA 90024	1
Dr. W. Destlar Dept. of Electrical Engineering University of Maryland College Park, MD 20742	1
Prof. R. Diament Columbia University Dept. of Electrical Engineering New York, NY 10027	1
Prof. W. Doggett NC State University P.O. Box 5342 Raleigh, NC 27650	1
Dr. H. Dreicer Plasma Physics Division Los Alamos Scientific Lab. Los Alamos, NM 87544	1
Dr. A. Drobot Naval Research Laboratory Code 4790 (SAI) Washington, D.C. 30275	1
Prof. W. E. Drummond Austin Research Associates 1901 Rutland Drive Austin, TX 78758	1
Prof. H. H. Fleischmann Lab. for Plasma Studies and School of Applied and Engr. Physics Cornell University Ithaca, NY 14850	1
Dr. D. Eccleshall U.S. Army Ballistic Research Lab. Aberdeen Proving Ground, MD 21005	1
Dr. Barbara Epstein Sandia Laboratories Albuquerque, NM 87185	1
Dr. A. Fisher Physics Dept. University of California Irvine, CA 92664	1
Dr. R. J. Faehl Los Alamos Scientific Lab. Los Alamos, NM 87544	1
Dr. Leon Feinstein Science Applications, Inc. 5 Palo Alto Square Palo Alto, CA 94304	1
Dr. Franklin Felber Western Research Corporation 8616 Commerce Ave. San Diego, CA 92121	1
Dr. Richard Fernslor Code 4770 Naval Research Lab. 4555 Overlook Ave., S.W. Washington, D.C. 20375	1
Dr. Thomas Fessenden Lawrence Livermore National Lab. L-321 University of California Livermore, CA 94550	1

DISTRIBUTION (Cont.)

	Copies
Dr. Robert Fossum, Director DARPA 1400 Wilson Boulevard Arlington, VA 22209	1
Dr. H. Freund Naval Research Lab. Code 4790 4555 Overlook Ave., S.W. Washington, D.C. 20375	1
Dr. M. Friedman Code 4700.1 Naval Research Laboratory Washington, D.C. 20375	1
Dr. B. Godfrey Mission Res. Corp. 1400 San Mateo Blvd, S.E. Suite A Albuquerque, NM 87108	1
Dr. T. Godlove Office of Inertial Fusion U.S. Department of Energy Washington, D.C. 20545	1
Dr. Jeffry Golden Naval Research Laboratory Washington, D.C. 20375	1
Dr. S. Goldstein Jaycor (Code 4770) Naval Research Lab. Washington, D.C. 20375	1
Dr. Victor Granatstein Naval Research Lab. Washington, D.C. 20375	1
Dr. S. Graybill Harry Diamond Lab. 2800 Powder Mill Rd. Adelphi, MD 20783	1
Dr. Michael Greenspan McDonnell Douglas Corp. St. Louis, MO 63166	1
Dr. Robert Greig Naval Research Lab. (Code 4763) 4555 Overlook Ave., S.W. Washington, D.C. 20375	1
Dr. J.U. Guillory Jaycor 20050 Whiting St. Suite 500 Alexandria, VA 22304	1
Dr. Irving Haber Code 4790 Naval Research Lab. Washington, D.C. 20375	1
Prof. D. Hammer Lab. of Plasma Studies Cornell University Ithaca, NY 14850	1
Dr. Robert Hill Physics Division, #341 National Science Foundation Washington, D.C. 20550	1
Dr. J. L. Hirshfield Yale University Mason Laboratory 400 Temple Street New Haven, CT 06520	1
Dr. Richard Hubbard Code 4790 (Jaycor) Naval Research Lab. 4555 Overlook Ave., S.W. Washington, D.C. 20375	1
Dr. Bertram Hui Naval Research Lab. Code 4790 4555 Overlook Ave., S.W. Washington, D.C. 20375	1
Dr. S. Humphries Sandia Laboratories Albuquerque, NM 87115	1

DISTRIBUTION (Cont.)

	Copies
Dr. Robert Johnston Science Applications, Inc. 5 Palo Alto Square Palo Alto, CA 94304	1
Dr. Howard Jory Varian Associates, Bldg. 1 611 Hansen Way Palo Alto, CA 94303	1
Dr. Glenn Joyce Code 4790 Naval Research Lab. 4555 Overlook Ave., S.W Washington, D.C. 20375	1
Dr. Selig Kainer Naval Research Lab. 4555 Overlook Ave., S.W. Washington, D.C. 20375	1
Dr. C.A. Kapetanakos Plasma Physics Division Naval Research Laboratory Washington, D.C. 20375	1
Dr. Denis Keefe Lawrence Beskeley Lab. 1 Cyclotron Road Berkeley, CA 94720	1
Dr. Douglas Keeley Science Applications, Inc. 5 Palo Alto Square Palo Alto, CA 94304	1
Dr. Hogil Kim A & FR Div. Lawrence Berkeley Lab. Berkeley, CA 94720	1
Dr. Hong Chul Kim A & FR Div. Lawrence Berkeley Lab. Berkeley, CA 94720	1
Dr. Kwang Je Kim Bldg. 64 #223 A & FR Div. Lawrence Berkeley Lab. Berkeley, CA 94720	1
Dr. Jin Joong Kim North Carolina State University Raleigh, NC 27607	1
Prof. N. M. Kroll La Jolla Institutes P.O. Box 1434 La Jolla, CA 92038	1
Dr. M. Lampe Naval Research Lab. Code 4790 4555 Overlook Ave., S.W. Washington, D.C. 20375	1
Dr. L. J. Laslett Lawrence Berkeley Lab. 1 Cyclotron Road Berkeley, CA 96720	1
Dr. Y. Y. Lau Naval Research Lab. Code 4740 (SAI) 4555 Overlook Ave., S.W. Washington, D.C. 20375	1
Dr. Glen R. Lambertson Lawrence Berkeley Lab. 1 Cyclotron Road, Bldg. 47 Berkeley, CA 94720	1
Dr. J. Carl Leader McDonnell Douglas Corp. Box 516 St. Louis, MO 63166	1

DISTRIBUTION (Cont.)

	Copies
Dr. W. M. Manheimer Naval Research Lab. Code 4790 4555 Overlook Ave., S. W. Washington, D. C. 20375	1
Dr. Edward P. Lee Lawrence Livermore National Lab L-321 University of California Livermore, CA 94550	1
Dr. Ray Lemke Air Force Weapons Lab Kirtland Air Force Base Albuquerque, NM 87117	1
Dr. Anthony T. Lin University of California Los Angeles, CA 90024	1
Dr. C. S. Liu Dept. of Physics University of Maryland College Park, MD 20742	1
Dr. Tom Lockner Sandia Laboratories Albuquerque, NM 87115	1
Dr. Conrad Longmire Mission Research Corp. 735 State Street Santa Barbara, CA 93102	1
Prof. R. V. Lovelace School of Applied and Eng. Physics Cornell University Ithaca, NY 14853	1
Dr. Joseph A. Mangano DARPA 1400 Wilson Blvd. Arlington, VA 22209	1
Dr. James Mark L-477 Lawrence Livermore Lab Livermore, CA 94550	1
Dr. Jon A. Masamitsu Lawrence Livermore National Lab L-321 University of California Livermore, CA 94550	1
Dr. Bruce R. Miller Div. 5246 Sandia Laboratories Albuquerque, NM 87115	1
Dr. Melvin Month Department of Energy High Energy Physics Washington, D.C. 20545	1
Dr. Philip Morton Stanford Linear Accelerator Center P.O. Box 4349 Stanford, CA 94305	1
Dr. Don Murphy Naval Research Lab 4555 Overlook Ave., S.W. Washington, D.C. 20375	1
Dr. Won Namkung E. E. Department University of Maryland College Park, MD 20742	1
Prof. J. Nation Lab of Plasma Studies Cornell University Ithaca, NY 14850	1
Dr. V. Kelvin Neil Lawrence Livermore Nat'l Lab P.O. Box 808, L-321 Livermore, CA 94550	1

DISTRIBUTION (Cont.)

	Copies
Dr. Barry Newberger Mail Stop 608 Los Alamos National Lab Los Alamos, NM 87544	1
Dr. C. L. Olson Sandia Lab Albuquerque, NM 87115	1
Dr. Edward Ott Dept. of Physics University of Maryland College Park, MD 20742	1
Dr. Peter Palmadesso Bldg A50 #107 Naval Research Lab Washington, D.C. 20375	1
Dr. Ron Parkinson Science Applications, Inc. 1200 Prospect St. P.O. Box 2351 La Jolla, CA 92038	1
Dr. Richard Patrick AVCO - Everett Research Lab, Inc. 2385 Revere Beac Pkwy Everett, MA 02149	1
Dr. Robert Pechacek Naval Research Lab Code 4763 4555 Overlook Ave., S.W. Washington, D.C. 20375	1
Dr. Sam Penner National Bureau of Standards Bldg. 245 Washington, D.C. 20234	1
Dr. Michael Picone Naval Research Lab 4555 Overlook Ave., S.W. Washington, D.C. 20375	1
Dr. R. Post Lawrence Livermore Lab University of California P.O. Box 808 Livermore, CA 94550	1
Dr. D. S. Prono Lawrence Livermore Lab P.O. Box 808 Livermore, CA 94550	1
Dr. S. Putnam Physics Internal Co. 2700 Merced St. San Leandro, CA 94577	1
Dr. Sid Putnam Pulse Sciences, Inc. 1615 Broadway, Suite 610 Oakland, CA 94612	1
Dr. Michael Raleigh Naval Research Lab Code 4763 4555 Overlook Ave., S.W. Washington, D.C. 20375	1
Dr. M. E. Read Naval Research Lab Code 4740 4555 Overlook Ave., S.W. Washington, D.C. 20375	1
Prof. M. Reiser Dept. of Physics & Astronomy University of Maryland College Park, MD 20742	1
Dr. M. E. Rensink Lawrence Livermore Lab P.O. Box 808 Livermore, CA 94550	1
Dr. Moon-Jhong Rhee E. E. Department University of Maryland College Park, MD 20742	1

DISTRIBUTION (Cont.)

	Copies
Dr. C. W. Roberson Naval Research Lab Code 4740 4555 Overlook Ave., S.W. Washington, D.C. 20375	1
Dr. J. A. Rome Oak Ridge National Lab Oak Ridge, TN 37850	1
Dr. Marshall N. Rosenbluth University of Texas at Austin Inst. for Fusion Studies RLM 11.218 Austin, TX 78712	1
Prof. Norman Rostoker Dept. of Physics University of California Irvine, CA 92664	1
Dr. C. F. Sharn Naval Sea Systems Command Department of the Navy Washington, D. C. 20363	1
Prof. S. P. Schlesinger Columbia University Dept. of Electrical Engineering New York, NY 10027	1
Prof. George Schmidt Physics Dept. Stevens Institute of Technology Hoboken, NJ 07030	1
Dr. Andrew M. Sessler Lawrence Berkeley Lab Berkeley, CA 94720	1
Dr. J. D. Sethian Naval Research Lab Code 4762 Washington, D.C. 20375	1
Dr. William Sharp Naval Research Lab Code 4790 (SAI) 4555 Overlook Ave., S.W. Washington, D.C. 20375	1
Dr. D. Straw AFWL Kirtland AFB, NM 87117	1
Dr. John Siambis Science Applications, Inc. 5 Palo Alto Square Palo Alto, CA 94304	1
Dr. J. S. Silverstein Code 4740 (HDL) Naval Research Lab 4555 Overlook Ave., S.W. Washington, D.C. 20375	1
Dr. M. Lee Sloan Austin Research Associates, Inc. 1901 Rutland Drive Austin, Texas 78758	1
Dr. L. Smith Lawrence Berkeley Lab 1 Cyclotron Road Berkeley, CA 94770	1
Dr. Joel A. Snow Senior Technical Advisor Office of Energy Research U.S. Department of Energy, M.S. E084 Washington, D.C. 20585	1
Dr. Philip Sprangle Naval Research Lab Code 4790 4555 Overlook Ave., S.W. Washington, D.C. 20375	1

DISTRIBUTION (Cont.)

	Copies
Dr. Doug Strickland Naval Research Lab Code 4790 (Beers) 4555 Overlook Ave., S W. Washington, D.C. 20375	1
Dr. Charles D. Striffler E. E. Dept. Univ. of Maryland College Park, MD 20742	1
Prof. R. Sudan Lab of Plasma Studies Cornell University Ithaca, NY 14850	1
Dr. C. M. Tang Naval Research Lab Code 4790 4555 Overlook Ave., S.W. Washington, D.C. 20375	1
Dr. R. Temkin Plasma Fusion Center Massachusetts Institute of Technology Cambridge, MA 02139	1
Dr. Lester E. Thode Mail Stop 608 Los Alamos National Lab Los Alamos, NM 87544	1
Dr. James R. Thompson Austin Research Associate, Inc. 1901 Rutland Drive Austin, Texas 78758	1
Dr. D. Tidman Jaycor 205 S. Whiting St. Alexandria, VA 22304	1
Dr. A. W. Trivelpiece Science Applications, Inc. San Diego, CA 92123	1
Dr. John E. Walsh Department of Physics Dartmouth College Hanover, NH 03755	1
Dr. Wasneski Naval Air Systems Command Department of the Navy Washington, D.C. 20350	1
Dr. N. R. Vanderplaats Naval Research Laboratory Code 6805 4555 Overlook Ave., S. W. Washington, D.C. 20375	1
Lt. Col. W. Whitaker Defense Advanced Research Projects Agency 1400 Wilson Boulevard Arlington, VA 22209	1
Dr. Mark Wilson National Bureau of Standards Gaithersburg, MD 20760	1
Dr. Gerold Yonas Sandia Lab Albuquerque, NM 87115	1
Dr. Simon S. Yu Lawrence Livermore National Lab L-321 University of California Livermore, CA 94550	1
Defense Technical Information Center Cameron Station Alexandria, VA 22314	12
Internal distribution:	
R	1
R04	1
R40	1

DISTRIBUTION (Cont.)

	Copies
Internal Distribution (Cont.)	
R401	1
R43 (C. W. Lufcy)	1
R44 (T. F. Zien)	1
R45 (H. R. Riedl)	1
R13 (J. Forbes)	1
R41 (P. O. Hesse)	1
R41 (R. Cawley)	1
R41 (M. H. Cha)	1
R41 (H. C. Chen)	1
R41 (J. Y. Choe)	1
R41 (R. Fiorito)	1
R41 (O. F. Goktepe)	1
R41 (M. J. Rhee)	1
R41 (D. W. Rule)	1
R41 (Y. C. Song)	1
R41 (H. S. Uhm)	1
R43 (A. D. Krall)	1
F	1
F14 (H. C. Coward)	1
F40 (J. F. Cavanagh)	1
F10 (K. C. Baile)	1
F46 (D. G. Kirkpatrick)	1
F34 (R. A. Smith)	1
F34 (E. Nolting)	1
F34 (V. L. Kenyon)	1
F04 (M. F. Rose)	1
F34 (F. Sazama)	1
N14 (R. Biegalski)	1
E431	9
E432	3
E35	1

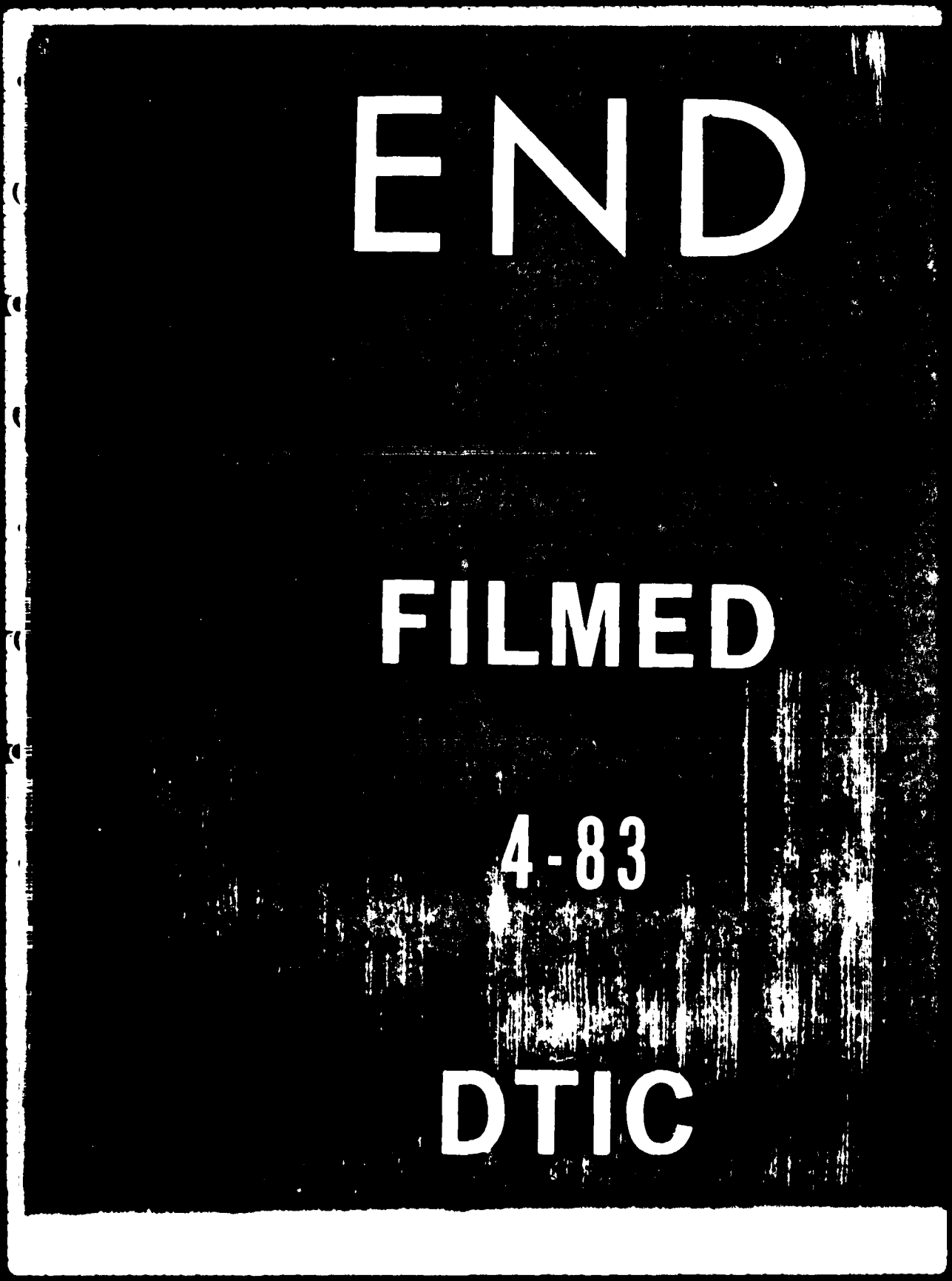
END
FILMED
4-83
DTIC